

Article

System-Level Operational and Adequacy Impact Assessment of Photovoltaic and Distributed Energy Storage, with Consideration of Inertial Constraints, Dynamic Reserve and Interconnection Flexibility

Lingxi Zhang ¹, Yutian Zhou ¹, Damian Flynn ², Joseph Mutale ¹ and Pierluigi Mancarella ^{1,3,*}

¹ School of Electrical and Electronic Engineering, University of Manchester, Manchester M13 9PL, UK; lingxi.zhang@manchester.ac.uk (L.Z.); yutian.zhou@manchester.ac.uk (Y.Z.); joseph.mutale@manchester.ac.uk (J.M.)

² School of Electrical and Electronic Engineering, University College Dublin, Dublin D04 V1W8, Ireland; damian.flynn@ucd.ie

³ Melbourne School of Engineering, University of Melbourne, Melbourne, VIC 3010, Australia

* Correspondence: pierluigi.mancarella@unimelb.edu.au or p.mancarella@manchester.ac.uk; Tel.: +44-7769-282384

Academic Editor: Gianfranco Chicco

Received: 1 June 2017; Accepted: 4 July 2017; Published: 13 July 2017

Abstract: The growing penetration of solar photovoltaic (PV) systems requires a fundamental understanding of its impact at a system-level. Furthermore, distributed energy storage (DES) technologies, such as batteries, are attracting great interest owing to their ability to provide support to systems with large-scale renewable generation, such as PV. In this light, the system-level impacts of PV and DES are assessed from both operational and adequacy perspectives. Different control strategies for DES are proposed, namely: (1) centralised, to support system operation in the presence of increasing requirements on system ramping and frequency control; and (2) decentralised, to maximise the harnessing of solar energy from individual households while storing electricity generated by PV panels to provide system capacity on request. The operational impacts are assessed by deploying a multi-service unit commitment model with consideration of inertial constraints, dynamic reserve allocation, and interconnection flexibility, while the impacts on adequacy of supply are analysed by assessing the capacity credit of PV and DES through different metrics. The models developed are then applied to different future scenarios for the Great Britain power system, whereby an electricity demand increase due to electrification is also considered. The numerical results highlight the importance of interconnectors to provide flexibility. On the other hand, provision of reserves, as opposed to energy arbitrage, from DES that are integrated into system operation is seen as the most effective contribution to improve system performance, which in turn also decreases the role of interconnectors. DES can also contribute to providing system capacity, but to an extent that is limited by their individual and aggregated energy availability under different control strategies.

Keywords: photovoltaic; distributed energy storage; inertia; system adequacy; renewable energy sources; interconnector

1. Introduction

The Paris Agreement aims to limit greenhouse gas emissions substantially in order to achieve the target of preventing global warming from being greater than 2 °C [1]. A substantial part of carbon emission is caused by the operation of fossil fuel power plants. Therefore, society is seeking alternative approaches to provide clean and low carbon energy. Renewable generation technologies

are recognised as one of the solutions towards a low carbon power system, while wind and solar photovoltaic (PV) generation are seen as key technologies within the potential renewable energy portfolio worldwide. Taking Great Britain (GB) as an example, due to various incentives, the installed wind and PV capacities have exceeded 15 and 10 GW, respectively, by the middle of 2016 [2], and they are expected to reach close to 48 and 34 GW, respectively, by 2035 [3]. The levelised costs of electricity from wind and solar generation have dropped by more than 30% and 80% respectively in the last eight years, which makes them more attractive technologies to achieve the ambitious emission reduction targets [4]. However, both technologies have certain drawbacks, such as the partial uncertainty and variability of power output, which requires more flexibility from the system to cope with their variable generation. For example, PV generation has some specific characteristics, such as diurnal availability, i.e., no generation at night and rapid output changes at dawn and dusk periods, that need to be properly dealt with. At high PV penetration levels, these characteristics of PV generation may threaten secure power system operation and consequently lead to renewable generation curtailment. In this context, it is key to both system operators and energy policy makers to develop a fundamental understanding of all the challenges and potential benefits associated with high penetration of renewables in the future, with regards to both system operation and security of supply. Furthermore, distributed energy storage (DES) technologies, such as batteries, are also attracting great interest because of their declining cost, an increasing requirement for operational flexibility and the potential to complement PV production. Hence, it is also crucially important to understand and quantify to what extent DES is capable of supporting power system development and operation alongside PV.

While extensive research has been carried out regarding the impacts of wind generation in the GB, much less attention has been paid to PV and, in general, to its implications at the system level. In fact, the majority of research on PV has focussed on optimal operation of PV systems either at a household level for the purpose of maximising consumer benefits [5,6], or at a medium/low voltage level in order to improve the performance of distribution networks (e.g., reducing line losses [7] and fluctuating feed-in power from PV systems [8]). However, there have been only a few studies [9–12] that have investigated and discussed the system-level implications of integrating a large volume of PV generation, in terms of the operation of an actual power system and the contribution to security of supply.

More specifically, large-scale PV installations can give rise to the so-called “duck curve” in the system net demand, which would increase the system ramping requirements to compensate for the diurnal variability of PV generation [13]. In the case of the GB system, the largest reduction of net demand caused by PV generation has reached 7.5 GW in 2016, which is equivalent to $\approx 70\%$ of the total installed PV capacity [14]. This implies that the 40 GW PV generation capacity projected for 2035 might impose a net demand reduction close to 28 GW, without operational measures in place, which consequently could cause critical issues for system operation. This is because a significant reduction in net demand usually occurs around midday (in summer) when the underlying demand has already been at a relatively low level. Meanwhile, not only relatively inflexible nuclear power plants would be challenged to stay online as base load generators, but also part-loaded combined cycle gas turbines (CCGT) would need to be capable of providing different reserve services. Consequently, the minimum stable output of these conventional generators might substantially limit the system’s capability to accommodate the power generated by PV and/or wind farms, although some nuclear plants could be constrained off to increase renewable energy integration. It is, therefore, of particular interest to investigate how different options, such as utilising energy storage and interconnectors, or scheduling methods could support system operation and integrate more renewable generation. Moreover, due to the operational displacement of conventional synchronous generation, the overall inertia of the system is declining significantly, which would increase the system frequency response requirement [15]. On the other hand, the surge of such requirements could in turn call for new operational constraints for existing generators to stay online to maintain the inertia level, which could in turn increase curtailment of renewable generation in a system lacking flexibility. Therefore, some publications have investigated

the flexibility contribution of interconnectors between adjacent grids [16–18]. In addition, different reserve allocation methods have been discussed in order to improve the integration of renewable energy sources [19,20]. Furthermore, several methods have been proposed to increase system flexibility and provide ancillary services from energy storage [21–24].

In parallel to the above operational issues, it is also crucial to understand from a planning perspective how PV generation can provide long-term security and contribute to a system's adequacy of supply. To this end, "capacity credit" is a classic measurement of the contribution of a technology to system adequacy. There have been several studies focusing on evaluating the capacity credit of PV [25–28]. However, these studies generally did not envisage specific situations, such as for the GB system, where the annual peak demand would occur on a winter evening when in fact PV generation is not available at all. Hence, DES systems could become of great interest to potentially enable PV to contribute to the supply at peak demand times, and therefore to system adequacy. On the other hand, DES systems could also be controlled to provide various services (e.g., reserves and frequency response) to support system operation, and at the same time, potentially, system capacity. In this light, it is of great interest to evaluate the capacity credit of coordinated operation of DES and PV systems, as well as the capacity credit of DES systems when providing operational support.

On the above basis, the primary aims of this paper, which are also its main novelty and contributions, are to: (i) analyse the system-level implications of high penetration levels of RES in both operational and planning terms, while considering primary frequency response requirements and contributions taking into account inertial constraints; (ii) develop a dynamic reserve allocation method to improve system flexibility; (iii) investigate the flexibility contribution from interconnectors in support of system operation; (iv) assess the potential for DES to support PV-rich system operation and enable PV generation to contribute to system adequacy; and (v) investigate the potential benefits from system-oriented DES operation in terms of energy and ancillary services provision beyond PV coordination. To these ends, models of different DES control strategies in both centralised and decentralised contexts, dynamic reserve allocation, and interconnector flexibility have been developed and integrated into a multi-service unit commitment model to perform time-series analysis of system operation. The system-level operational implications of PV and DES are investigated in terms of wind curtailment and energy imported from or exported to the interconnected systems. Furthermore, a framework for assessing the capacity credit of DES and PV systems under different control strategies is developed to investigate the system-level impacts on adequacy of supply, which includes definitions of four different capacity credit metrics and the corresponding assessment algorithms. A possible increase in system demand, due to future electrification in heating and transportation sectors, is also considered by using relevant models of electric heat pumps (EHP) and electric vehicles (EV) in [27] and [29], respectively.

The remainder of the paper is structured as follows: Section 2 introduces models that have been developed for DES control, dynamic reserve allocation and interconnector flexibility, as well as the adopted models for the multi-service unit commitment and future electricity demand; additionally, the corresponding methodologies utilised for capacity credit assessment are also described in Section 2; Section 3 presents case studies focusing on the future GB system and the results are demonstrated and discussed in Section 4. Finally, conclusions are summarised in Section 5. Supplementary information is also provided as an Appendix A at the end of the paper.

2. Models and Methodology

2.1. Future Demand Modelling

A breakdown of the expected residential electricity consumption in GB until 2035 is depicted in Figure 1 [3]. The reduction in appliance and lighting loads is caused by improvements in technology energy efficiency, while the overall increase in electricity demand is primarily due to a growth in electric vehicles and electric heat pumps.

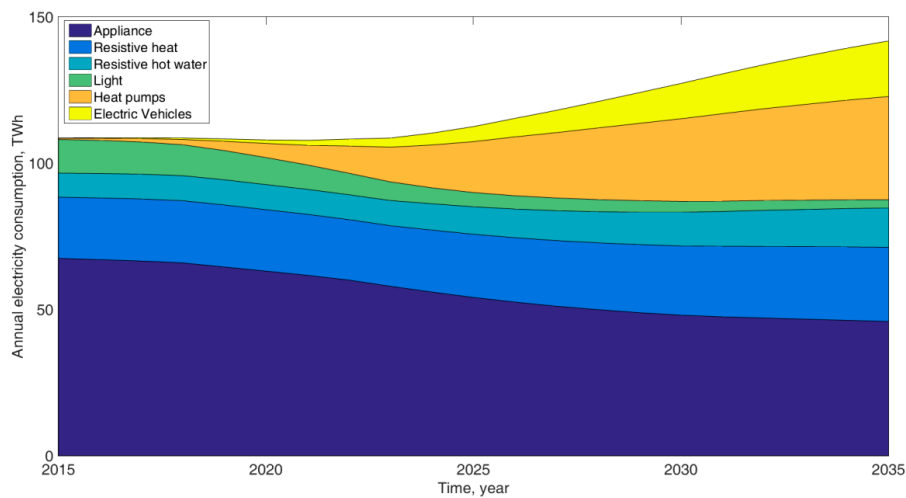


Figure 1. Residential sector annual demand breakdown for Great Britain [3].

As for the system studies of this paper, it is important to understand the shape of the future system profiles (particularly at low and peak demands), such that bottom-up methods have been built for the corresponding time-series energy consumption profile for future scenarios. More specifically, a high resolution multi-energy model [29] is applied to estimate residential dwelling energy consumption, and then the overall energy demand is appropriately re-scaled based on the annual energy consumption given in [3]. The EHP operation profile follows the modelling described in [3], while for EV charging profiles the occupancy profile generated in the multi-energy model is applied to EV modelling using a similar control logic as in [30]. Therefore, the future system demand (D_t^F) can be calculated from the current demand (D_t^C), appliance energy reduction (d_t^{Ap}), demand from EHPs (d_t^{EHP}) and energy consumption of EVs (d_t^{EV}), as seen in Equation (1):

$$D_t^F = D_t^C - d_t^{Ap} + d_t^{EHP} + d_t^{EV} \quad (1)$$

2.2. System Operational Model

Power system operation is simulated using the linear programming (LP) unit commitment (UC) model introduced in [31]. The model is well suited for flexibility studies and exhibits excellent computational performance relative to other traditional models but without losing significant scheduling accuracy, as demonstrated in [31]. As key points, the model considers the primary frequency response, and secondary and tertiary upward and downward reserves in the unit commitment. It is critical to include the primary frequency response provision rate and tertiary reserve constraints; in fact, the provision rate of primary frequency response can increase in a low-inertia power system in order to satisfy the frequency nadir constraint, while the requirement for tertiary reserves (i.e., short term operating reserve—STOR—in GB) can increase due to uncertainty and variability of renewable generation on the relevant timescale. In addition, new “cross-service” constraints can arise in the system, such as provision of inertial response from online generators that are committed to provide tertiary reserve. The original constraints of the model from [31] are explained in Appendix A. Details of extensions to the original model are provided below, which account for new inertial response requirements and constraints.

2.3. Assessment and Modelling of Primary Frequency Response Requirements with Inertial Considerations

The frequency variation of a system is associated with the system inertia and the mismatch between generation and demand, such as due to a sudden demand surge or generation loss. In this case, primary frequency response (PFR) is activated in order to confine the variation of system frequency and

recover it to a normal range within a pre-set timeframe. Many publications, even recent ones, on UC research do not consider a PFR constraint [24,32–34] or only consider a total PFR requirement instead of linking the PFR provision rate requirement with system inertia in UC optimisation [31]. Considering the high penetration level of non-synchronous RES which can result in a low-inertia system [35] and the increment of the largest generation loss due to the construction of nuclear plant in the future, both PFR provision rate and full requirement are expected to have a substantial increase (however, the requirements for PFR could potentially be reduced if nuclear plants are incentivised to operate in part-loaded mode). Therefore, it is necessary to explicitly implement, in the UC model, both inertial constraints and PFR provision rate constraints in order to accurately capture the operation of future low-carbon power systems. Since the PFR is assumed to be solely provided by conventional generators, focusing on a generation loss at each simulation time step (t), the change in frequency ($\Delta f_{t+\tau}^{sys}$) in sub-time-step (τ) following a generation loss (P_t^{loss}) at the beginning of a time step is calculated in (2), with corresponding system stored rotational energy (E_t^{sys}), load damping rate (Dpr), system demand level (D_t), conventional generator output ($p_{n,t}^{con}$). The system stored energy is calculated in (3) based on the ratings (p_n^{conMax} , p_s^{phsMax}) of synchronous conventional generators and pumped hydro storage (PHS), the average ratio of active power to apparent power equipment rating (β^{pf}), the corresponding inertial constants for each unit (H_n^{con} , H_s^{phs}), and the number of online units ($U_{n,t}^{con}$, $U_{s,t}^{phs}$):

$$2 \cdot \frac{E_t^{sys}}{f_{t+0}^{sys}} \cdot \frac{\partial \Delta f_{t+\tau}^{sys}}{\partial \tau} + Dpr \cdot D_t \cdot \Delta f_{t+\tau}^{sys} = \sum_{n \in N} [p_{n,t+\tau}^{con} - p_{n,t+0}^{con}] - P_t^{loss} \quad (2)$$

$$E_t^{sys} = \left[\sum_{n \in N} (P_n^{conMax} \cdot H_n^{con} \cdot U_{n,t}^{con}) + \sum_{s \in S} (P_s^{phsMax} \cdot H_s^{phs} \cdot U_{s,t}^{phs}) - P^{lossMax} \cdot H^{loss} \right] \cdot \frac{1}{\beta^{pf}} \quad (3)$$

Currently, three metrics are usually considered to assess the frequency response performance of a system, namely the (initial) rate of change of frequency (RoCoF), frequency nadir, and quasi-steady-state (QSS) frequency [15]; the corresponding constraints in a unit commitment model are discussed in [15] and illustrated below for clarity. The RoCoF is often used by generators (including embedded generation) to trigger grid disconnection for self-protection in the case of (islanding) contingencies. Therefore, it is necessary to confine the system stored energy value above a certain level, so that the frequency variation in the initial stage following (maximum online) generation loss is slower than the RoCoF setting. It must be emphasised that the maximum online generation loss is considered as a constant parameter, which equals the capacity of the largest inflexible nuclear plant. Although the largest infeed loss of the system might actually change, for example due to fault, scheduled maintenance or even inflexible plant shutting down due to lack of flexibility, in this paper nuclear plants are considered as “must-run” units at full output, following the current approach by National Grid. Another major contingency might be caused by loss of an interconnector; however, this does not correspond to the potentially largest infeed loss, as the interconnection GB-France has two independent 1000 MW circuits and it is unlikely to experience a simultaneously breakdown of both transmission lines. Further, the loss of a high voltage, direct current (HVDC) interconnector would not bring about loss of inertia, so again this contingency would likely have less impact than the loss of the largest online generator. The relevant constraint based on RoCoF setting ($ROCOF^{Max}$) is shown in Equation (4) with the maximum generation loss ($P^{lossMax}$), system nominal frequency (f_{t+0}^{sys}) and its corresponding unit inertial value (H^{loss}). The primary frequency response provision rate requirement (frr_t) due to the nadir constraint is presented in (5). The purpose of this constraint is to ensure that the system frequency trajectory lies above the nadir set by the system operator. The derivation detail of Equation (5) is explained in [15]. In this paper, it is assumed that the PFR is solely contributed by the governor droop response and no response contribution from static resources (e.g., HVDC link) has been considered. T^d is the delivery time of the PFR from conventional generators, while Δf_{db} is the deadband before triggering of PFR. The last constraint relating to PFR is the quasi-steady-state

condition. As shown in (6), it ensures that the system has procured sufficient PFR to recover the frequency back to an acceptable level ($\Delta f^{QSS_{Max}}$) after the full deployment of PFR, and so that the secondary response can securely take over frequency recovery. In constraint (6), the total PFR provision capacity is calculated by the provision rate multiplying the corresponding delivery time, with the assumption that the convention generators have a constant ramp rate in the transient period of PFR deployment:

$$ROCOF^{Max} \geq \frac{P^{loss_{Max}} \cdot f_{t+0}^{sys}}{2 \cdot E_t^{sys}} \tag{4}$$

$$\Delta f^{Nadir} \geq \frac{P^{loss_{MAX}}}{Dpr \cdot D_t} + \frac{2frr_t \cdot E_t^{sys}}{(Dpr \cdot D_t)^2 \cdot f_{t+0}^{sys}} \ln \left(\frac{2frr_t \cdot E_t^{sys}}{f_{t+0}^{sys} \cdot Dpr \cdot D_t \cdot (P^{loss_{MAX}} - Dpr \cdot D_t \cdot \Delta f^{db}) + 2frr_t \cdot E_t^{sys}} \right) \tag{5}$$

$$frr_t \cdot T_d \geq P^{loss_{Max}} - \Delta f^{QSS_{Max}} \cdot Dpr \cdot D_t \tag{6}$$

Since the PFR provision rate requirement and (online) system stored energy are both variables in Equation (5), certain techniques need to be applied in order to convert this non-linear constraint into a linear one, which can subsequently reduce the computational time. The method applied in [15] uses additional binary variables and constraints, which would lead to a significant computational time increase and it is consequently not suitable for scenario analyses. Therefore, an alternative iterative approach is proposed here, which is depicted in Figure 2. In Equation (5), the PFR provision rate requirement (frr_t) and the system stored rotational energy (E_t^{sys}) are the only two variables, which are mutually dependent on each other. Therefore, an initial static PFR provision rate requirement is used in the UC to simulate system operation. Then, the value of stored energy is post-assessed and applied to Equation (5) in order to determine the corresponding PFR provision rate requirement. Subsequently, this dynamic rate requirement is used again in the UC model and simulations are re-run. After a few iterations, both the PFR provision rate and system inertia tend to converge to the optimal level, as illustrated in Figures 3 and 4. The iterations are terminated when the difference between successive rounds for the system operational cost is smaller than a pre-set value.

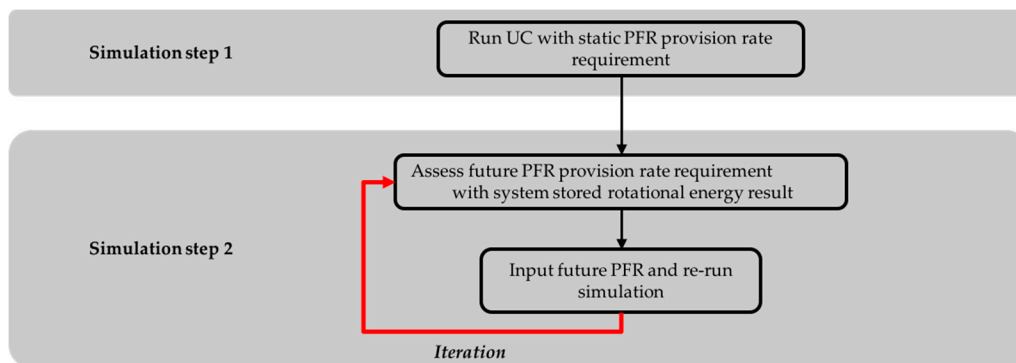


Figure 2. PFR calculation iteration approach, with inertial consideration.

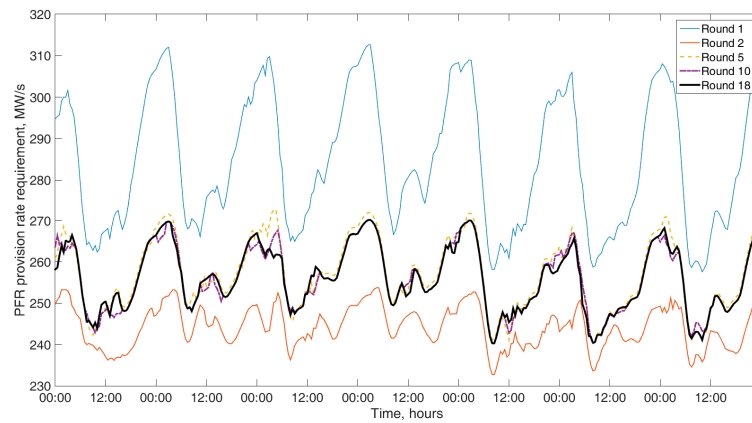


Figure 3. PFR provision rate requirement across a week in an iterative process.

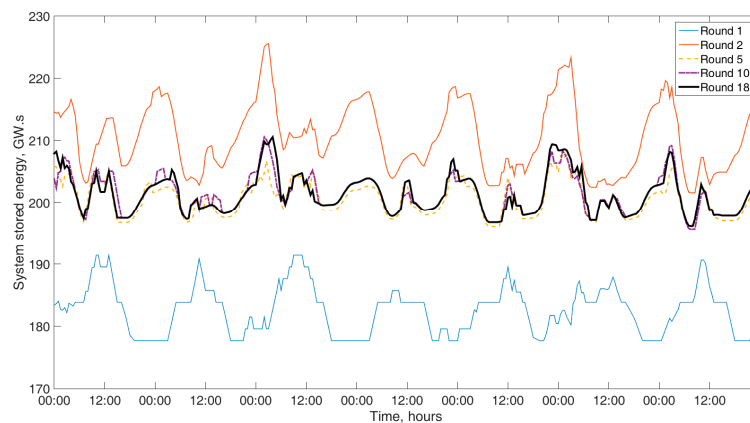


Figure 4. System stored rotational energy across a week in an iterative process.

2.4. Dynamic Reserve

In traditional power systems, the penetration of renewable energy resources is relatively low and the system is scheduled to integrate all renewable generation. In addition, certain volumes of spinning and standing reserves are required to deal with the sudden loss of power plants and the uncertainty and variability of the underlying demand and renewable energy sources. This “static” secondary and tertiary reserves requirement ($R_{i,t}$) is often calculated based on the maximum conventional generator capacity ($P^{lossMax}$), forecasted demand, wind and solar output, and standard deviation of the demand, wind and solar forecast errors ($\delta^{D/W/S}$), as shown in Equation (7) [36,37]. The forecast errors of PV, wind and demand are considered to be following a normal distribution. A “3-sigma” rule is applied to demand and solar reserve calculation, while “3.5-sigma” is considered in order to cover the forecast error of wind generation, based on the information shown in [38]:

$$R_{i,t} = P^{lossMax} + \sqrt{(3 \cdot PV_t \cdot \delta_t^S)^2 + (3 \cdot D_t \cdot \delta_t^D)^2 + (3.5 \cdot W_t \cdot \delta_t^W)^2} \quad (7)$$

However, the installed capacity of (variable) renewable energy resources is increasing substantially, which leads to a significant increase in the required amount of reserve with longer time scales (i.e., STOR in GB, which has 4 h delivery time and 2 h full delivery requirement). For example, the standard deviation of the wind generation forecast error is 9.3% for 4 h ahead if adopting the data presented in [38]. Then, the maximum value of the STOR required by wind generation, which is calculated in Equation (7) can reach 32% of the wind forecasted output. Considering that the installed wind capacity is 48 GW in National Grid’s 2035 Gone Green scenario [3], consequently the system might

require some 15 GW (32% of 48 GW) of conventional generation to provide STOR to handle wind uncertainty. This would lead to a shortage of flexibility in a system with total conventional capacity (excluding nuclear) of only 39 GW (however, reserve could be provided by other components, such as pumped hydroelectric storage, demand response and interconnector, etc.). In fact, even assuming a state of the art wind forecasting technique, the system may experience some periods with insufficient reserve provision capability, as, for example, shown by the one week simulation results of GB system in Figure 5, with the installed renewable capacities given in National Grid 2035 Gone Green scenario. More specifically, in Figure 5, there are a few hours when the renewable production is higher than the system demand. Meanwhile, the total requirement for frequency response and upward reserves even exceeds the headroom (“headroom” here refers to as the sum of spare capacity of online generators for ramping up and the capacity of standing generators, such as offline open cycle gas turbine (OCGT) and CCGT, which can achieve a quick start-up to provide upward reserve. However, ramp rates have not been considered, which makes the considered headroom to be the actual maximum ramp-up potential of the supply system) of the generation portfolio. If no measure has been taken, the security constraints of the supply system may be compromised due to a lack of flexibility. Therefore it is necessary to reassess or increase (although nuclear plants are considered as must-run units in this paper, it is also possible to shut down nuclear plants and switch on more flexible plants to increase the total “online” flexibility of the system) the flexibility contribution from each component to satisfy the flexibility requirement of the system.

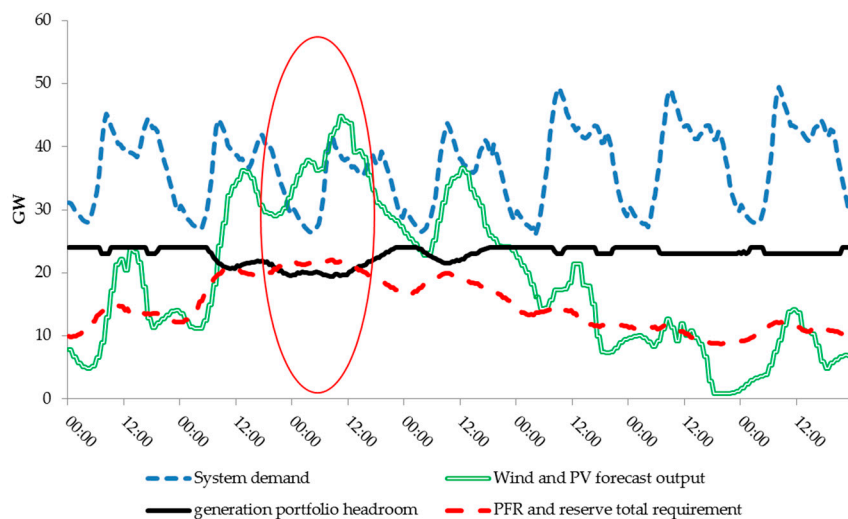


Figure 5. Example of insufficient reserve capacity during high PV and wind generation and low load period in National Grid 2035 Gone Green scenario.

Therefore, a new dynamic reserve modelling method is proposed to release part of the system flexibility at high renewable energy penetration levels. First of all, the proposed reserve method is only applied to the wind reserve component in Equation (7), because the wind farms are more geographically concentrated, compared with the PV plants, and most of them are connected to the transmission network, which can give the system operator direct control over the wind curtailment beforehand based on system operational conditions. The system operator may decide to curtail wind to reduce the reserve provision from conventional generators and minimise the operational cost, or it may curtail wind as a last resort to avoid infeasible scheduling as mentioned above due to a lack of flexibility. The output of wind farms (w_t) that can be securely integrated is calculated based on the wind forecast potential output (W_t) and time-ahead curtailment (ω_t) in Equation (8). Instead of using the wind forecast output to calculate the secondary and tertiary reserves requirement, the wind output that can be integrated is applied in Equation (9) to determine the system reserve requirement,

which would allow the system operator to find a balance between reserve provision and renewable integration to minimise the system operational cost:

$$w_t = W_t - \omega_t \quad (8)$$

$$R_{i,t} = P^{lossMax} + \sqrt{(3 \cdot PV_t \cdot \delta_i^S)^2 + (3 \cdot D_t \cdot \delta_i^D)^2 + (3.5 \cdot w_t \cdot \delta_i^W)^2} \quad (9)$$

2.5. Interconnectors

Interconnectors are a key potential flexibility provider by importing/exporting electricity from/to adjacent grids when needed. Moreover, interconnection capacity is rapidly increasing (for example, GB is projected to install another 19 GW of interconnectors in addition to current 4 GW capacity by 2035 [3]), which makes its modelling (and that of neighbouring systems) essential in UC, and its specific modelling is another new contribution of this paper. The interconnectors are based on voltage source or current source converter technologies. Without entering specific technical details of each specific interconnector and without loss of generality, we model the different interconnectors as one equivalent interconnection element as a combination of generation and demand. This is because we are primarily interested in the energy flexibility that imports and exports can contribute to the system. The net output of the interconnector to the system (p_t^{int}) is calculated with individual interconnectors import ($p_{l,t}^{int_{im}}$) and export ($p_{l,t}^{int_{ex}}$) flows, as in (10). The import and export flows are constrained by the interconnector capacity (p^{intMAX}), import/export capacity limits ($CL^{int_{im}}$, $CL^{int_{ex}}$) and by its current mode ($bn_{l,t}^{int}$) (binary variable, 1 represents import mode and 0 represents export mode), as shown in Equations (11) and (12) respectively. The import and export flow is also limited by the ramping rate of the interconnectors represented by Equations (13) and (14):

$$p_t^{int} = \sum_{l \in L} (p_{l,t}^{int_{im}} - p_{l,t}^{int_{ex}}) \quad (10)$$

$$p_{l,t}^{int_{im}} \leq p^{intMax} \cdot CL^{int_{im}} \cdot bn_{l,t}^{int} \quad (11)$$

$$p_{l,t}^{int_{ex}} \leq p^{intMAX} \cdot CL^{int_{ex}} \cdot (1 - bn_{l,t}^{int}) \quad (12)$$

$$\left| p_{l,t}^{int_{im}} - p_{l,t-1}^{int_{im}} \right| \leq RAMP_l^{int} \quad (13)$$

$$\left| p_{l,t}^{int_{ex}} - p_{l,t-1}^{int_{ex}} \right| \leq RAMP_l^{int} \quad (14)$$

2.6. Distributed Energy Storage

Higher penetration levels of RES in the future will call for more system flexibility. Besides the existing large scale pumped-hydro storage, DES can also be deployed to provide flexibility, and may be coupled with PV panels. The fundamental functionality of DES can be characterised by the following parameters including the state of charge, charging/discharging power rates, charging/discharging efficiencies, maximum charging/discharging power ratings, energy capacity, and minimum energy level. Existing typical control algorithms implemented in DES aim to maximise the self-consumption of PV generation within individual dwellings. However, with future extensive installation of communication infrastructures, system operators could be able to coordinate the operation of batteries to absorb renewable generation production and provide ancillary services, enabling them to contribute to system operation. The following subsections thus introduce the basic models that describe the operation of DES, the current independent control algorithm focusing on local energy consumption, and an integrated control to maximise the benefits of battery utilisation at the system level.

2.6.1. Basic Model of DES

Modelling of DES to provide energy arbitrage to support system operation is included here, which is developed based on the storage model in [39]. The energy of DES ($e_{m,t}^{DES}$) is calculated in (15) with its instantaneous charging rate ($p_{m,t}^{DES_c}$), discharging power ($p_{m,t}^{DES_{dc}}$), charging and discharging efficiency ($\eta^{DES_c}, \eta^{DES_{dc}}$) and the simulation time step length (Δ^{ts}). Equation (16) determines the energy level of DES ($e_{m,t}^{DES}$), which is confined within its energy capacity ($E^{DES_{Max}}$ and $E^{DES_{Min}}$). The charging and discharging power of DES is also limited by its power rating ($P^{DES_{Max}}$) and current state variable ($bn_{m,t}^{DES}$), which is a binary, and uses 1 and 0 to represent the charging or discharging state of DES, as shown in Equations (17) and (18):

$$e_{m,t}^{DES} - e_{m,t-1}^{DES} = \left(p_{m,t}^{DES_c} \cdot \eta^{DES_c} - \frac{p_{m,t}^{DES_{dc}}}{\eta^{DES_{dc}}} \right) \cdot \Delta^{ts} \quad (15)$$

$$E_m^{DES_{Min}} \leq e_{m,t}^{DES} \leq E_m^{DES_{Max}} \quad (16)$$

$$p_{m,t}^{DES_c} \leq P^{DES_{Max}} \cdot bn_{m,t}^{DES} \quad (17)$$

$$p_{m,t}^{DES_{dc}} \leq P^{DES_{Max}} \cdot (1 - bn_{m,t}^{DES}) \quad (18)$$

2.6.2. Independent Control Strategy

In the residential sector at a household level, consumers with PV panels on their rooftops can be motivated to also install DES for the primary purpose of maximising the self-consumption of the energy generated by PV panels, for instance to maximise savings on electricity bills; and if there is spare capacity left after maximising the self-consumption, the DES can also be used to minimise local network injections to avoid voltage issues in distribution networks. Furthermore, in regions such as GB, where solar PV cannot contribute to the supply of system peak demands (usually in winter evenings), distributed DES could potentially be coordinated with and signalled by the system operator to store the solar energy generated in the daytime so as to supply system peak demands in the evening periods, leading to a peak clipping effect and a contribution to generation capacity. This coordinated control aims to represent how PV and DES could be controlled to displace conventional generation capacity. It is worth noting that the peak clipping operation of combined DES and PV panels is typically only needed by the system operator for a certain number of days throughout a year, in the case of GB it will be several days during winter. In summary, consumers with PV panels could operate their DES to achieve the following objectives:

- Maximising their self-consumption of solar PV energy at a household level;
- Minimising the maximum feed-in power of solar PV at a household level;
- Contributing to generation capacity by shifting the generation from solar PV to supply the system demand at peak times.

As the aforementioned control strategy of DES does not recognise the operation of other generation technologies, this control strategy is referred to here as “Independent control”. Figure 6 demonstrates the control strategy and how it is integrated into the UC model and capacity credit assessment.

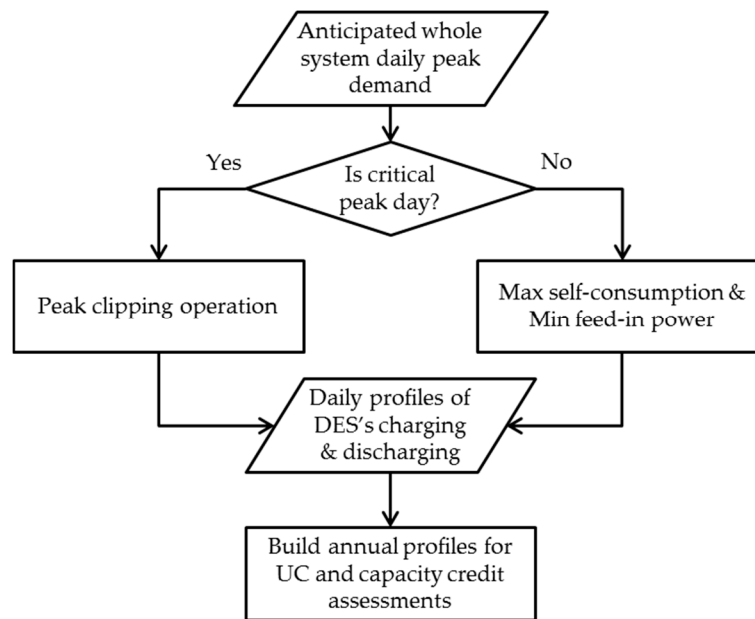


Figure 6. Methodology for integrating “independent control” strategy into the UC model and capacity credit assessment.

More specifically, the peak clipping operation and the joint maximisation of self-consumption and minimisation of power injection are optimised on a daily basis.

Peak Clipping Operation

In terms of the “peak clipping operation”, DES is modelled by an aggregated storage system with the assumption that all the DES would be well coordinated by signals from the system operator based on the total system demand. In this light, the following dual-stage optimisation formulation is proposed for utilisation of solar PV to contribute to the system demand at peak times, which is developed based on the relevant optimisation in [39,40]. The first stage in Equations (19) and (20) determines the minimum daily peak demand that can be achieved, while the second stage minimises the energy charged to achieve the minimum daily peak demand.

The daily peak demand K in Equation (19) is minimised subject to constraints (15)–(18) and (20) where T represents the number of time segments per day, so that the minimum daily peak demand (denoted later by K^*) can be determined:

$$K_m^* = \text{Min}_{t \in T} : K_m \quad (19)$$

$$K_m > K_{m,t}^{\text{Original}} - p_{m,t}^{\text{DES}_{dc}} \quad \forall t \in T \quad (20)$$

In the second stage, the energy charged to achieve the minimum daily peak demand K^* is then minimised, while K^* becomes a constraint for the net demand. To this end, the objective function in (21) is minimised subject to the constraints in Equations (15)–(18) and (22):

$$\text{Min} : \sum_{t \in T} \left(p_{m,t}^{\text{DES}_{dc}} \cdot \Delta t^s \right) \quad (21)$$

$$K_{m,t}^{\text{Original}} - p_{m,t}^{\text{DES}_{dc}} < K_m^* \quad \forall t \in T \quad (22)$$

As mentioned in [40], although the economic aspects have not been explicitly modelled, the above optimisation is in line with realistic commercial arrangements (e.g., the capacity payments proposed in

the GB electricity market reform [41]) that might be available to incentivise consumers with batteries and PV panels to shift PV generation to supply the demand at peak times, while the minimisation in the second stage is also in line with the minimisation of the potential system cost for deploying these resources (this is because the extra solar PV energy shifted could not further reduce the peak demand and thus bring no additional contribution to generation capacity; however, it would cause more energy losses and unnecessary economic penalties to the consumers).

Self-Consumption Maximisation and Power Injection Minimisation

With regards to the maximisation of solar PV self-consumption and minimisation of power injection from PV panels, another dual-stage optimisation is proposed as follows. In the first stage, the solar PV self-consumption is maximised by minimising the electricity consumption from the grid side, as the objective function in Equation (23). This objective function is minimised subject to Equations (24) and (15)–(18). Unlike the optimisation in Equations (19) and (20), all the demand, charging/discharging power, generation of PV panels, and storage parameters are for an individual household, rather than an aggregated storage:

$$\text{Min} : \sum_{t \in T} (p_{m,t}^G \cdot \Delta^{ts}) \quad (23)$$

$$p_{m,t}^G \geq \max \left(K_{m,t}^{\text{Original}} - P_{m,t}^{\text{PV}} - p_{m,t}^{\text{DESc}} + p_{m,t}^{\text{DESc}}, 0 \right) \quad \forall t \in T \quad (24)$$

In the second stage, the maximum feed-in power p^{MFI} in Equation (25) is minimised subject to Equations (15)–(18), (24) and (26)–(27). Note that the solution of the objective function in Equation (23) (denoted as e^{G^*} i.e., the daily minimum energy consumed from the grid side) is used as a constraint in Equation (26). The constraint in Equation (26) ensures that the primary objective for this control is to maximise the self-consumption of solar PV, whereas the minimisation of power injection from PV panels is only carried out if there is spare energy capacity:

$$p_m^{MFI} = \text{Min} : p_{m,t}^{FI} \quad (25)$$

$$\sum_{t \in T} (p_{m,t}^G \cdot \Delta^{ts}) \leq e^{G^*} \quad (26)$$

$$p_{m,t}^{FI} \geq \max \left(P_{m,t}^{\text{PV}} - K_{m,t}^{\text{Original}} + p_{m,t}^{\text{DESc}} - p_{m,t}^{\text{DESc}}, 0 \right) \quad \forall t \in T \quad (27)$$

2.6.3. Integrated Control Strategy

An “integrated” control is finally proposed here, whereby DES operation is simultaneously optimised with the UC simulation to provide system operational support, which could be facilitated in the future by aggregators, for example.

In this “integrated” control, the generation scheduling of conventional power plants is co-optimised with DES operation to reduce the system operational cost. Since the operation of batteries is coordinated by the system operator, it allows the batteries to be charged with electricity not only generated by roof-top PV panels but also from other sources in the grid, such as wind farms, conventional generators and interconnectors, which could lead to batteries providing grid support.

The total capacity of batteries is projected to exponentially increase to 2.62 GW in GB by 2035 [3]. This high capacity could potentially allow DES to provide ancillary services at an aggregated level under what we called “Integrated” control.

The capability of a battery to provide secondary and tertiary reserves is constrained by two factors. The first one is its energy capacity. The deployment of upward reserve provision ($r_{m,i,t}^{\text{DES}up}$) from DES is accomplished by a continuous discharging of pre-stored energy and vice versa for downward reserve ($r_{m,i,t}^{\text{DES}dn}$), as calculated in Equations (28) and (29). The minimum deployment duration of each reserve

service (Δ_i^r) is also considered in Equations (28) and (29). Therefore, the energy capacity within a DES can be split into four parts, as shown in Figure 7a. The residual energy of DES available for discharging and upward reserve, while spare capacity for charging and downward reserve are co-optimised in the scheduling process. The second factor is the available power capacity. The mechanism is illustrated in Figure 7b, as increasing the charging or discharging power output of a DES reduces the corresponding downward or upward reserve provision capacity. This mutually exclusive relationship of upward and downward frequency response, reserve provision and energy arbitrage are constrained in Equations (30) and (31) respectively, while it is also limited by the maximum percentage of DES capacity for service provision (RP^{DES}):

$$\sum_{i \in I} (r_{m,i,t}^{DES_{up}} \cdot \Delta_i^r) \leq e_{m,t}^{DES} - E^{DES_{Min}} \tag{28}$$

$$\sum_{i \in I} (r_{m,i,t}^{DES_{dn}} \cdot \Delta_i^r) \leq E^{DES_{Max}} - e_{m,t}^{DES} \tag{29}$$

$$\sum_{i \in I} (r_{m,i,t}^{DES_{up}}) \leq \min(P^{DES_{Max}} \cdot (1 - bn_{m,t}^{DES}) - p_{m,t}^{DES_{dc}} + p_{m,t}^{DES_{dc}}, P^{DES_{Max}} \cdot RP^{DES}) \tag{30}$$

$$\sum_{i \in I} (r_{m,i,t}^{DES_{dn}}) \leq \min(P^{DES_{Max}} \cdot bn_{m,t}^{DES} - p_{m,t}^{DES_{dc}} + p_{m,t}^{DES_{dc}}, P^{DES_{Max}} \cdot RP^{DES}) \tag{31}$$

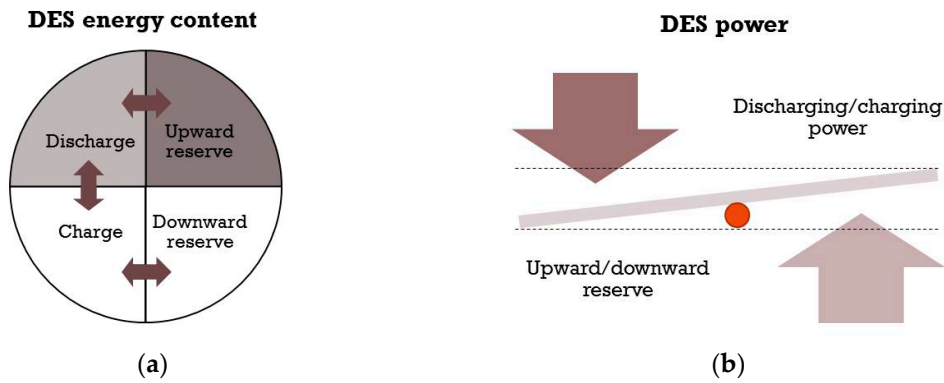


Figure 7. (a) DES energy balance between energy arbitrage and ancillary service provision; (b) DES power balance between energy arbitrage and ancillary service provision.

2.7. Framework for Capacity Credit Assessment

Besides short-term operational issues, as discussed above, it has also been pointed out earlier that in some regions, such as GB, solar PV may not be able to support long-term security and contribute to system adequacy from a planning perspective. For instance, in the case of GB, as seen in Figure 8, when the system demand reaches its peak value (in winter evenings) there is normally no available PV generation. In this context, DES systems can be incentivised to enable solar PV to supply the demand at peak times, as illustrated in Figure 8. Thus, unlike the capacity credit of solar PV that has been defined and assessed in [40], this paper makes consideration for the capacity credit of solar PV that is enabled by DES systems.

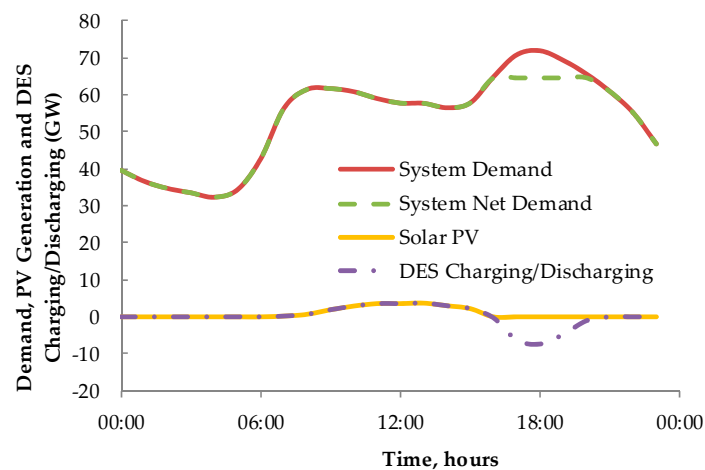


Figure 8. Demonstration of the peak clipping control of DES and PV in the future GB system.

More specifically, through the “independent” control model proposed in Section 2.6.2, PV systems may be enabled to provide system capacity at peak times through the peak clipping control of DES systems, as again illustrated in Figure 8. Additionally, in terms of the “integrated” control model developed in Section 2.6.3, there might also be an intrinsic contribution from DES systems to adequacy of supply, depending on the discharging behaviour of DES systems at system peak times. For example, in a certain scenario, as seen in Figure 9, there is a clear and continuous DES discharging during the peak demand period under “Integrated” control, while DES is charged between midnight and 5:00 by using excess wind generation to reduce energy exports/curtailments.

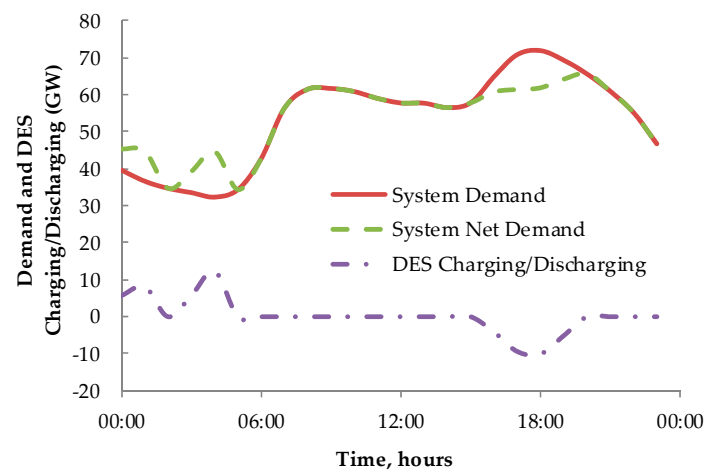


Figure 9. Demonstration of “integrated” control of DES and PV in the future GB system.

This DES discharging leads to a direct peak reduction in the system net demand and thus a contribution to system capacity. In this light, it also becomes of great interest to quantify this intrinsic capacity credit of DES systems while they are operated to provide different system services, such as secondary and tertiary reserve and frequency response, etc. [42]. On the above basis, four capacity credit metrics are adopted to assess the DES-oriented capacity contribution from different control strategies for DES and PV systems. The four capacity credit metrics are defined in detail based on the definitions in the framework for capacity credit assessment developed in [40], and summarised below. It is also worth noting that the capacity contribution is essentially enabled by deploying DES, regardless of the control strategies. In this context, the capacity credit is generally defined for the DES-enabled system without referring to a specific control strategy. For instance, the DES-enabled

system can represent the coordinated DES and PV systems, as in “independent” control, or the DES systems that are controlled and signalled by the system operator to provide various services to improve system flexibility, as in “integrated” control.

- Effective load carrying capability (ELCC): as seen in Figure 10a, this metric measures the capacity credit of the DES-enabled system as the amount of additional demand that can be supplied by the system with DES without compromising the adequacy level of the system without DES. The ELCC metric directly represents the additional demand that can be supplied by deploying the DES-enabled system.
- Equivalent firm capacity (EFC): as shown in Figure 10b, this metric expresses the capacity credit of the DES-enabled system as the equivalent capacity of a perfectly reliable generator. Basically, the EFC estimates the amount of perfectly reliable capacity added to the system without DES in order to achieve the same adequacy level of the system with DES. The EFC metric represents the capacity contribution as an equivalent generation capacity without being affected by specific reliability characteristics attached to a certain type of generation.
- Equivalent conventional capacity (ECC): according to Figure 10, unlike the EFC, this metric evaluates the capacity credit of the DES-enabled system as the equivalent capacity of a real conventional generator. More specifically, a real conventional generator is added to the system without DES to maintain the corresponding adequacy level the same as the one of the system with DES. The added capacity of the real conventional generator is the ECC of the DES-enabled system, as represented by the intersection point of Curve (A) and the LOLF (loss of load frequency) of the system with DES in Figure 10c. As a further point, the real conventional generator may not be able to quantify the ECC of a DES-enabled system, due to its own reliability characteristics. This is the case represented by Curve (B) in Figure 10c, where a less reliable generator is used.
- Equivalent generation capacity substituted (EGCS): as illustrated in Figure 10d, this metric quantifies directly the amount of existing conventional generation capacity that can be displaced by the DES-enabled system, without compromising the adequacy level of the system without DES. The EGCS metric indicates the capability of the DES-enabled system to displace existing generation capacity.

Note that in Figure 10 the classical reliability indicator, loss of load frequency (LOLF), is used to represent the level of adequacy in the capacity credit definitions and it is also used later in the case studies, even though other indicators could be used [40].

According to the definitions of the capacity credit metrics as demonstrated in Figure 10, specific searching algorithms can be used to determine the numerical values of these metrics, as developed in [40]. For instance, a bisection searching algorithm can be used to find the numerical values of the ELCC, EFC and ECC metrics, while the EGCS metric can be calculated by using a heuristic searching algorithm.

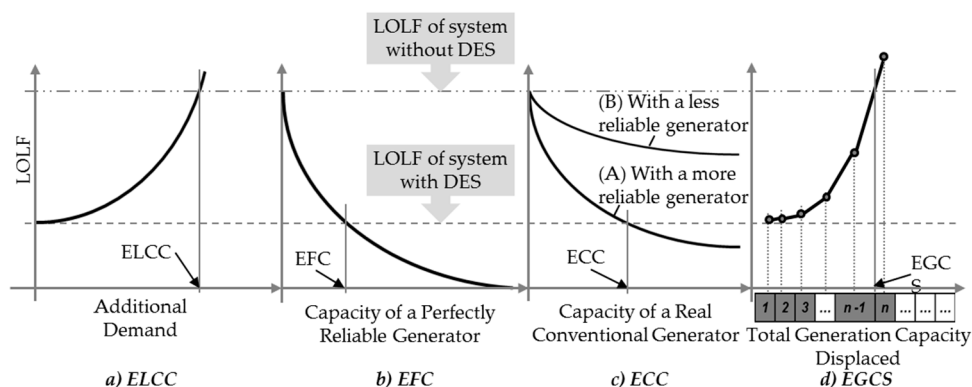


Figure 10. Conceptual illustration of the definitions of different capacity credit metrics.

Figure 11 shows a general algorithm for assessing the capacity credit metrics, whereas the detailed calculation algorithms are presented in Figure 12. It should be noted that in order to take proper account of the chronological correlations across DES operation, renewable and conventional generation the underlying reliability assessment is carried out by running sequential Monte-Carlo simulation (SMCS).

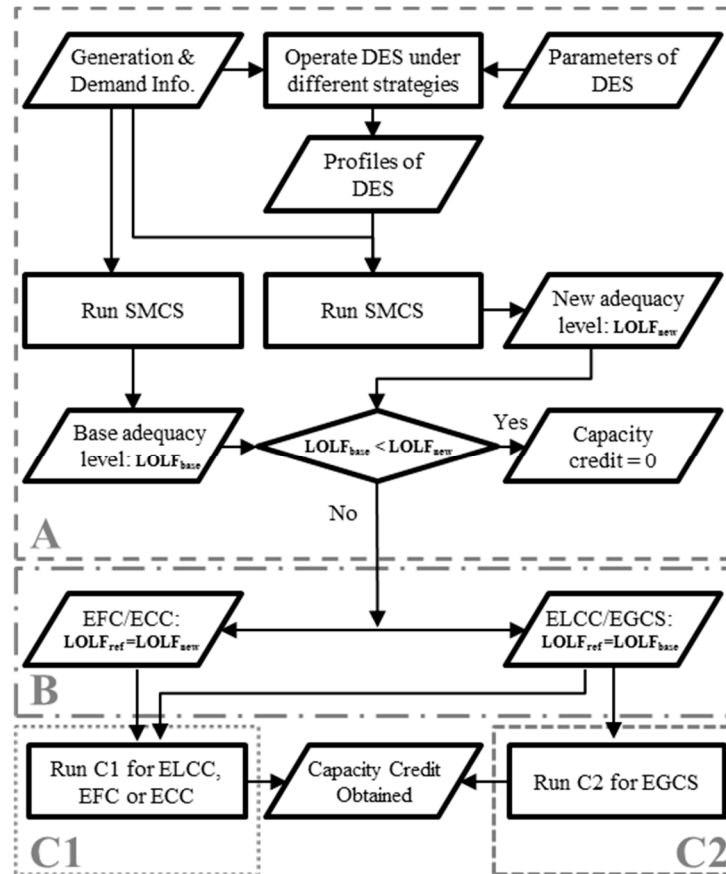


Figure 11. General algorithm for capacity credit assessment.

More specifically, Block A in Figure 11 calculates the two adequacy levels that are used as references in Figure 10, i.e., the LOLFs of systems with and without DES. It is clear that the capacity credit is zero if the LOLF of system with DES is greater than the LOLF of the system without DES. Depending on the capacity credit metric assessed, Block B in Figure 11 chooses the reference adequacy level, which will be used in the searching process in Blocks C1 and C2.

The searching algorithms are further explained in Figure 12. Figure 12a shows bisection searching to calculate the value of ELCC, EFC and ECC, respectively. The grey shaded parts in Figure 12a are used differently depending on whether ELCC (with a virtual load) or EFC/ECC (with a virtual generator) is calculated. In Figure 12a, γ is the iterative capacity value, while γ_{\max} and γ_{\min} mark the search interval. When assessing ECC, the benchmark unit needs to be checked ex ante whether it is able to measure the ECC and also an initial searching interval could be given accordingly. The accuracy of the bisection searching is denoted by ε (set here to 2%). The heuristic searching algorithm for the EGCS metric is shown in Figure 12b, which represents the procedure illustrated in Figure 10d. In the end, the value of EGCS is obtained via linear interpolation of the points $(C_{n-1}, \text{LOLF}_{n-1})$ and (C_n, LOLF_n) , where C_n refers to the total displaced generation capacity in round n and LOLF_n is the corresponding adequacy level.

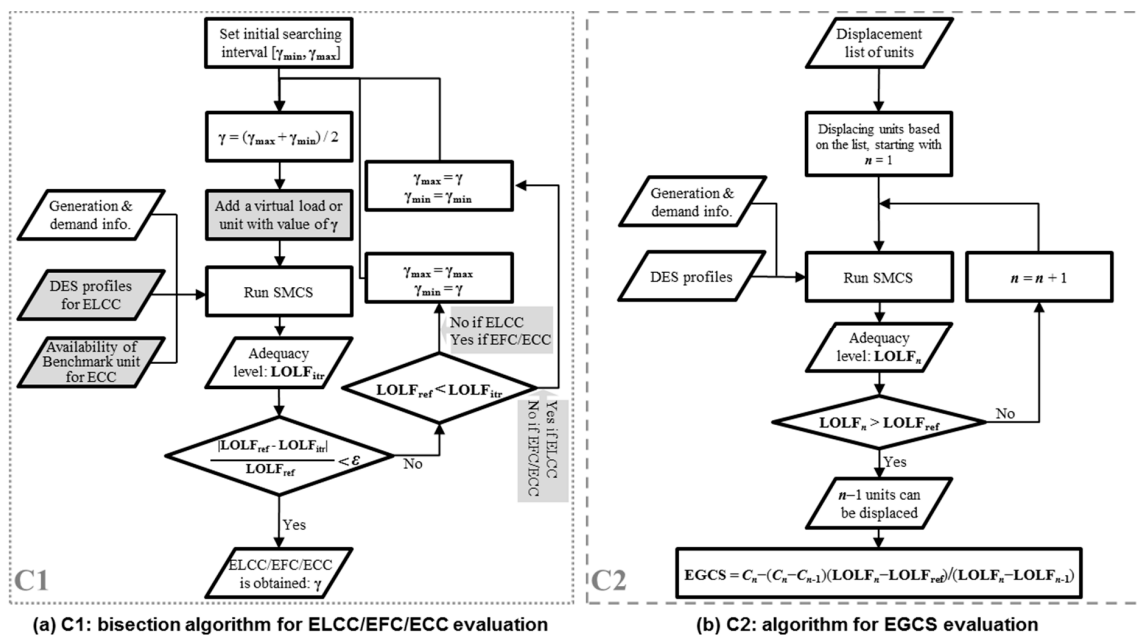


Figure 12. Searching algorithms for capacity credit calculation.

3. Case Study Description

3.1. System Description

The GB grid in 2035 from the Gone Green scenario in the National Grid report is used as the test system, with the corresponding capacity configuration given in Table 1 [3]. The reason for choosing Gone Green scenario among all four scenarios in [3] is that this scenario is created to specifically represent a high penetration of renewable energy sources. The characteristics of conventional generators are detailed in [31]. The largest generator loss is set to 1.8 GW, which is also used in [15]. The RoCoF limit is set to 0.5 Hz/s based on information [43] given by office of gas and electricity markets (Ofgem). The inertia constants of nuclear, gas, steam and hydro turbines are set to 5, 4, 3, and 3 MW·s/MVA respectively, retrieved from [44]. The average value of the ratio MW (rating)/MVA (rating) is assumed to be 0.8 for the stored rotational energy calculation. The GB wind and solar generation profiles are generated from the models introduced in [45], which is based on the PV and wind farms distribution in 11 GB regions and the corresponding wind speed and irradiance data. The United Kingdom government has only released construction plans for 13.7 GW interconnectors, as shown in Table 2. Therefore the interconnectors are classified into two types: one to the EU main continent countries with nuclear based generation and the other one to Ireland and Nordic countries with renewable based power plants. Then, the corresponding interconnectors are aggregated and scaled up to the capacity level mentioned in Table 1. The DES investigated in this paper is assumed to be a domestic battery. Each battery is assumed to be coupled with a 4 kW PV panel, while the power rating and energy capacity (in the case study, the energy capacity is used as a reference for battery installation expansion) of a battery are 5 kW and 10 kWh respectively with 90% round-trip efficiency, which is the average specification of a Tesla Powerwall 1 and 2 (however, domestic batteries may have better performance in the future with regards to efficiency, power and energy ratings, etc. In this paper, the current specification is applied for 2035 scenario simulation). However, the PFR deployment time of conventional generators are set to 10 s, as given in [15]. During the simulation, a small penalty is attached to PV curtailment in the cost function, so that wind curtailment (it needs to be acknowledged that it is feasible to increase system flexibility by using pre-curtailed wind generation to provide ancillary services, but this discussion is out of scope for this paper) is prioritised, as necessary, which is consistent with the direct controllability of the system operator at transmission network level. Based on

all the simulations carried out in the following case studies, the maximum annual PV curtailment level is less than 0.1%. Therefore, only the wind curtailment figure is examined in the following discussions.

Table 1. System capacity information (retrieved from [3]).

Technology	Interconnector	Gas	Carbon Capture Storage	Biomass	Nuclear
Capacity (GW)	23.26	22.05	7.42	3.65	18.55
Technology	Pumped hydro storage	Wind	Solar	Solar battery	-
Capacity (GW)	2.1	48.1	34.6	2.62	-

Table 2. GB interconnector projection (retrieved from [46]).

Country	Name	Capacity (MW)	Commission Time
France	IFA	2000	existing
	Eleclink	1000	2019
	IFA2	1000	2020
	FAB link	1400	2020–2022
The Netherlands	BRITNED	1000	existing
Belgium	NEMO	1000	2019
Ireland and Northern Ireland	Moyle	500	existing
	East-West	500	existing
	Greenlink	500	2021
Norway	NSN	1400	2021
	North Connect	1400	2022
Denmark	Viking Link	1000	2022
Iceland	Ice Link	1000	2024

3.2. System Demand

The time-series demand profile increase/reduction due to electrification and appliance efficiency improvements is depicted in Figure 13. It can be seen that the electricity consumption of EHPs has an obvious seasonal variation with minor demand increase in the summer, while the load increase from EVs and reductions in appliance consumption are more constant across the year. By combining this additional demand with the current system demand recorded in [14], the resulting future load duration curve is shown in Figure 14 (the figure is plotted with the consideration that all RES could be integrated (i.e., there is no curtailment due to operational constraints), hence, in practice at periods of negative net demand, there can be some RES curtailments and/or export). Electrification increases the system peak load to 72 GW, consistent with National Grid's Gone Green scenario in [3]. It needs to be emphasised that these electrified demands may represent opportunities for demand response applications, which can help to reduce the system peak and improve the integration of renewable energy; however, this is not considered in this paper. Furthermore, as the capacity of conventional generators is only 50 GW in 2035, the system may have to heavily rely on electricity imports through interconnectors during peak periods in winter evenings, in the case of renewable generation also being at a low level; therefore, the system could face a shortage of supply when adjacent networks coincidentally have a peak demand. Moreover, the minimum system load is slightly reduced in 2035, as during the summer periods the reduction in appliance load can be higher than the load increase from EVs and EHPs. The resulting demand net of renewable generation (based on historical profiles) is also plotted in Figure 14. There are a few hundred hours with negative net demand, which requires generation curtailment, energy shifting or export to ensure secure system operation, while conventional generation is also required to be kept online to provide, for example, ancillary services.

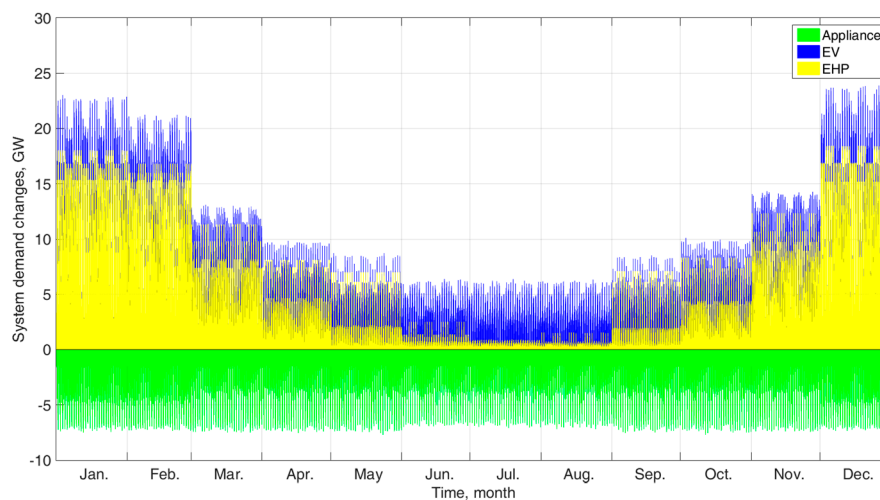


Figure 13. Estimated appliance load reduction and additional EV and EHP demands in the Gone Green scenario for the GB system in 2035.

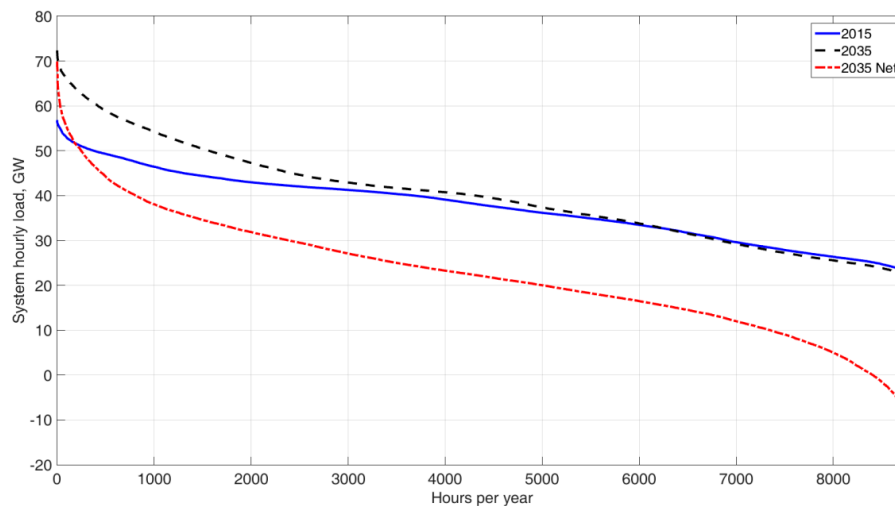


Figure 14. Estimated load duration curves of the GB system for 2015 and 2035 in Gone Green scenario.

3.3. Case Studies

- **PV penetration:** PV generation has some specific characteristics, such as the diurnal variation in the daytime and across seasons, etc. Therefore, it may limit the output of other generators and change the energy import and export. Therefore, the first case study is focussed on the PV penetration level. The performance of the system is investigated with regards to the energy production of different generation resources and interconnector utilisation. This analysis has been carried out for the installed PV capacity at the Gone Green level (referred as business as usual (BaU, the capacities of the generation portfolio adopted in the BaU scenario are the same as those in the National Grid Gone Green Scenario [3]. In addition, the BaU scenario does not consider the interconnection capacity limit and the service provision from batteries) and also with additional 5, 15, 25 and 35 GW of PV.
- **Interconnector flexibility:** Since the net demand (however, the scheduling needs to satisfy the security constraints, which would require the curtailment of renewable generation in the periods of negative demand) of GB system in 2035 could reach as low as -15 GW or up to 72 GW as shown in Figure 14, electricity import/export could be necessary to avoid load/renewable generation

curtailment. However, the import/export flow is controlled by the interconnectors and depends strongly on the operational state of adjacent grids. For example, in practice, the adjacent grids may not be able to supply/absorb the required energy and/or provide capacity support to the GB system via interconnectors. As the specific operation of adjacent networks is not simulated in the model, we have modelled potential interconnection operation through parametric flow constraints, simulating the GB system with BaU, 75%, 50%, 25% and 0% caps on the import/export capacity of the interconnectors. The capacities of the system generation portfolio are kept the same as the information shown in Table 1.

- **Battery integration:** The case studies for battery benefits are listed in Table 3. In “independent” and “integrated A”, simulations of system operation are carried out with additional 5, 15, 25, 35 and 45 GWh distributed batteries, while the functions considered for these batteries are energy arbitrage and peak clipping. Then, in the following “integrated B” case, the battery capacity is fixed at the Gone Green level with an additional 25 GWh in order to focus on examining the effect of different assumptions on battery capability to provide ancillary services. The possibility of secondary and tertiary reserve provision from batteries is investigated in “integrated B”. The reserve provision limits are set at 25%, 50%, 75% and 100% of total battery capacity, so that the system operator can optimise the ancillary service provision and energy arbitrage activities of the batteries.
- **Capacity credit:** The capacity credit of the combined storage and PV is evaluated for the following two control strategies: “independent control”; “integrated” control with a 50% battery capacity reserve provision limit imposed. Additionally, the capacity credit is also assessed for different battery penetration levels.

Table 3. Battery case study list.

Case No.	Energy Access Range		Battery Ancillary Service (Multiple)	
	PV	Whole System	Energy Arbitrage (Peak Clipping)	Secondary and Tertiary Reserves
Independent	✓		✓	
Integrated A		✓	✓	
Integrated B		✓	✓	✓

3.4. Simulation Setup

The simulation is carried out on a Matlab R2015a platform with an interface to the optimisation solver FICO XPRESS 7.6. The mixed integer programming (MIP) gap and the iteration convergence gap are both set to 0.5%. The time step of the simulation is set at half hour in order to include the deployment detail of secondary reserve, and each simulation includes 7 day profiles to ensure that the operation of pumped hydro storage is properly captured. The computer used for running the simulation has an 8 core CPU with 3.7 GHz clock speed and 32 GB random-access memory, while the computational time of a single yearly simulation is 2 h.

4. Results and Analysis

4.1. PV Penetration

The generation mix of the system and the monthly export energy with different PV capacities are shown in Figures 15 and 16.

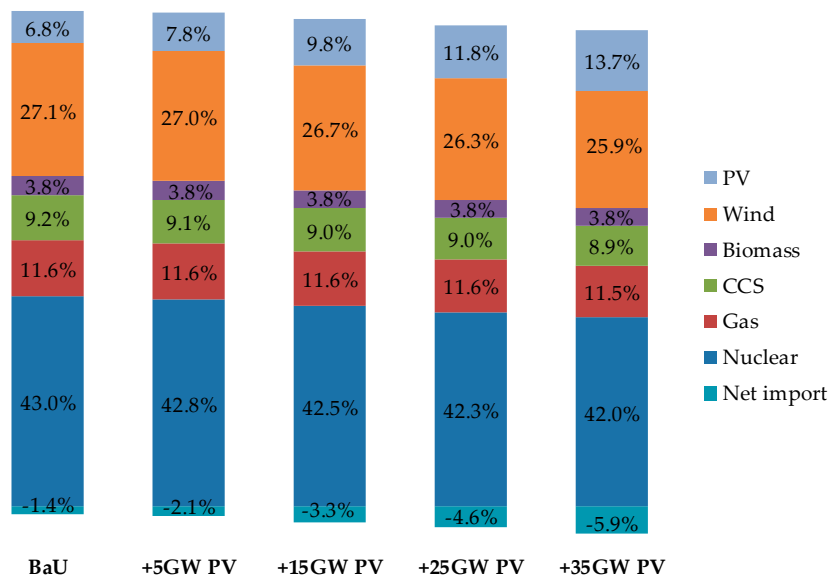


Figure 15. System annual generation output breakdown in scenarios with different PV penetration levels.

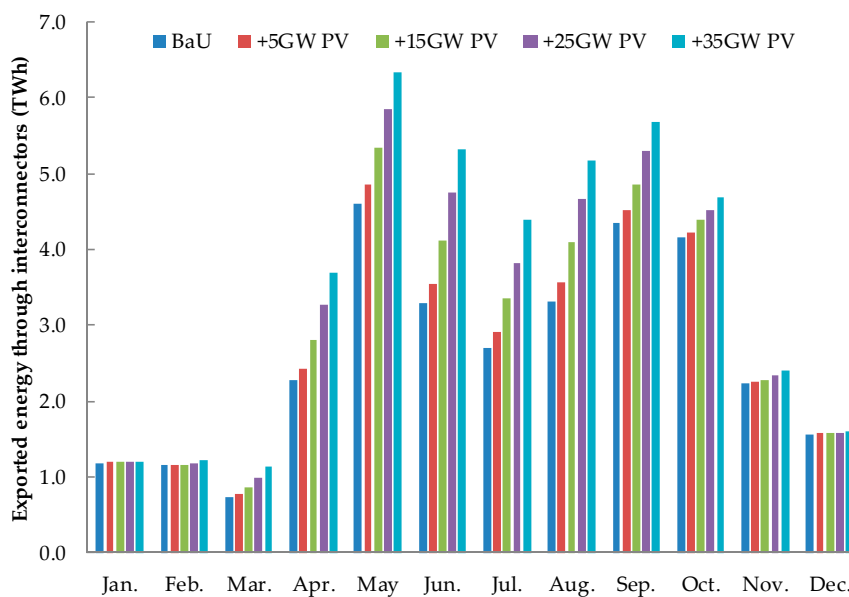


Figure 16. Total export energy for each month with additional PV capacity.

In Figure 15, it can be seen that the GB system shifts from net import to net export, as the net export energy percentage is 1.4% relative to the annual demand in the BaU case. With additional PV installation, the net export energy percentage is further increased from 1.4% to 5.9%. In addition, the wind and nuclear generation production mixes are also slightly reduced by 1.2% and 1% respectively in comparison with BaU and an extra 35 GW PV cases. The net export increase should be interpreted as a combination of reduced import and greater export energy flow volumes. In particular, as shown in Figure 16, system exports tend to increase during the summer but remain at a constant level in winter with additional PV capacity. This is because the system has a high demand in the winter with low PV generation, which allows the system to fully accommodate the extra solar generation without resorting to interconnection flexibility.

4.2. Interconnection Flexibility

Table 4 shows the number of hours when the aggregated interconnector flow reaches the specific capacity limits. It can be seen that for most time periods the import power is less than 25% of the aggregated interconnection capacity, as there are only 23 h with the import capacity reaching 25% in the year. In addition, the number of hours when the import power reached the imposed 50%, 75% limits and full capacity are all the same as the 25% case, which is 23 h. This indicates that the GB system has around 23 h with a high conventional generation capacity shortage in 2035 and it needs to rely on electricity import from adjacent grids to ensure secure operation.

Table 4. Number of hours of aggregated interconnector's import/export power reaching specific capacity limit.

Limit Reached (Number of Hours)	Capacity Limit Imposed				
	100%	75%	50%	25%	>0%
Import	23	23	23	23	3189
Export	14	157.5	637	1935	4616

With regard to the export operation of the interconnectors, the export power only reaches 50% of the aggregated interconnection capacity for 637 h in a year. The interconnector operates in an export mode more frequently than an import mode, which sustained 4616 hours and 3189 h respectively as shown in Table 4.

Figure 17 shows the cumulative number of hours of the aggregated interconnector working in import, export or no exchange modes. The system is exporting electricity most of the time between midnight and dawn, which is coincident with high wind generation periods. On the other hand, the aggregated interconnector is mostly operating in import mode during the evening peak, which highlights the necessity of including interconnection in the generation portfolio. During daytime, the export and import periods are more equally split depending on the capacity of installed renewable generation.

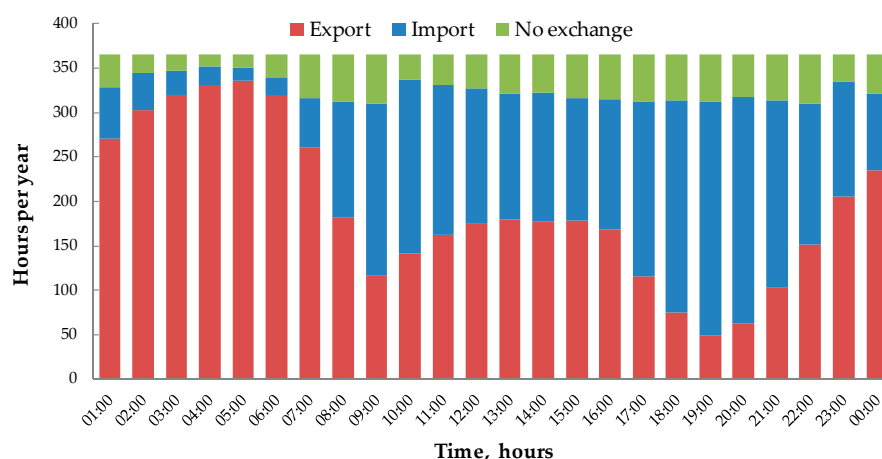


Figure 17. Interconnection import/export number of hours for different periods of the day in a year.

Figure 18 compares the system generation output characteristics between the BaU case (with fully available interconnection) and the 0% interconnection capacity availability case. The results in terms of renewable generation production indicate that, while the PV output does not change, more wind output is curtailed, making the wind generation contribution decrease from 27.1% to 19.4%. The output level of flexible conventional generators (i.e., biomass, CCS plants and gas turbines) increases from 3.8%, 9.2% and 11.6% to 4.9%, 11.4% and 16.3% respectively, while the generation contribution from

inflexible nuclear plants decreases from 43% to 41.3%. This is because the system requires more conventional generators to provide extra flexibility when the interconnection is unavailable.

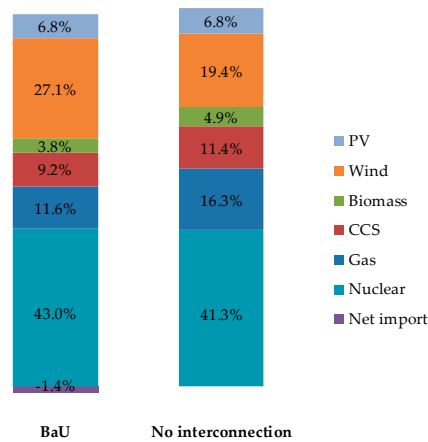


Figure 18. System annual generation output breakdown in the BaU and no-interconnection scenarios.

4.3. Battery Integration

4.3.1. Control Approach Comparison

First of all, the annual wind curtailment, import and export energy of the system with different control strategies and penetration levels are illustrated in Figure 19. This figure shows that annual wind curtailment, import and export energy remain roughly the same even with higher battery installation in “independent” control. This occurs because the energy access range is limited to electricity generated by rooftop PV panels. However, extending the energy access range to the whole system does not substantially improve wind integration level under the current system operational constraints (generator ramping limits, minimum up and down times, start up and shut down process, etc.—details are provided in Appendix A), as seen by the results of “integrated A”. This highlights the fact that the system is lacking sufficient flexibility to provide ancillary services in order to safely integrate this additional renewable generation and the current intervention taken by the system operator is to curtail the wind generation. With regard to import and export energy in the “integrated A” case, they both decrease with more battery storage, as batteries are charged with excess renewable generation and discharged at peak hours later to support the system, which leads to a reduction in renewable generation export and electricity import during system peak periods.

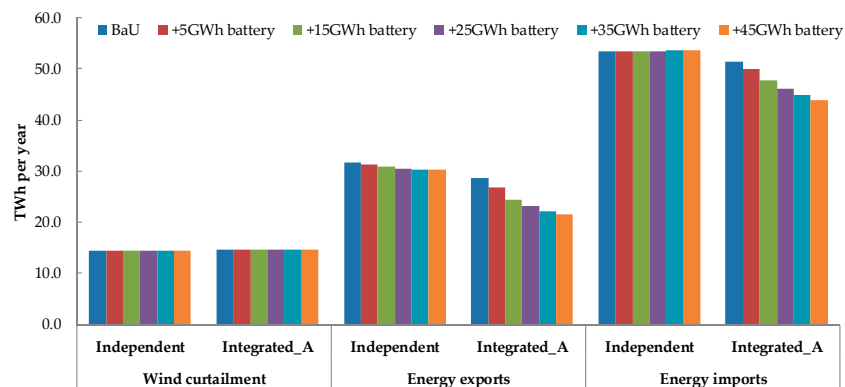


Figure 19. Annual wind curtailment, export and import energy with different battery installation capacities (“independent” and “integrated A” control strategies).

4.3.2. Battery Multiple-Functions

As mentioned above, the system may require ancillary service provision from batteries at given times to support further renewable integration. Therefore, in “integrated B” scenario we investigate the benefits of multiple services provision from batteries, namely, secondary and tertiary upward and downward reserve provision. The resulting annual wind curtailment and import and export energy for the system are shown in Figure 20. It can be seen that wind curtailment is significantly reduced with a higher reserve provision capability allowance and the lowest level of wind curtailment is only 1 TWh compared with 14.6 TWh in the BaU case. This supports the conclusion, given in Section 4.3.1, that the limitation for wind integration is caused by a lack of system flexibility in terms of ancillary services. However, further changes in wind curtailment, import and export energy are negligible when the maximum reserve provision capability of the batteries is extended beyond 50% of the battery total capacity, as shown in Figure 20. Further, increasing wind integration also leads to a reduction in import energy and an increase of export energy, as again seen in Figure 20, which means that less flexibility from interconnectors is required. The contributions from different technologies on secondary and tertiary upward reserve requirement are depicted in Figures 21 and 22. The conventional generators are gradually relieved from secondary upward reserve provision, as the spinning reserve percentage is reduced from 84% to 63% as shown in Figure 21. Moreover, it can be seen in Figure 22 that more tertiary reserve provision is contributed by spinning conventional generators and batteries, which both increase by 6% in the 100% reserve case compared with the BaU case.

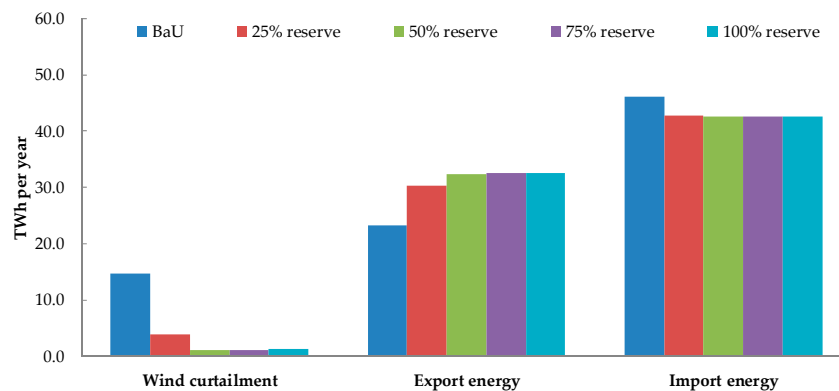


Figure 20. Annual wind curtailment, export and import energy with different battery service provision limits (“integrated B”).

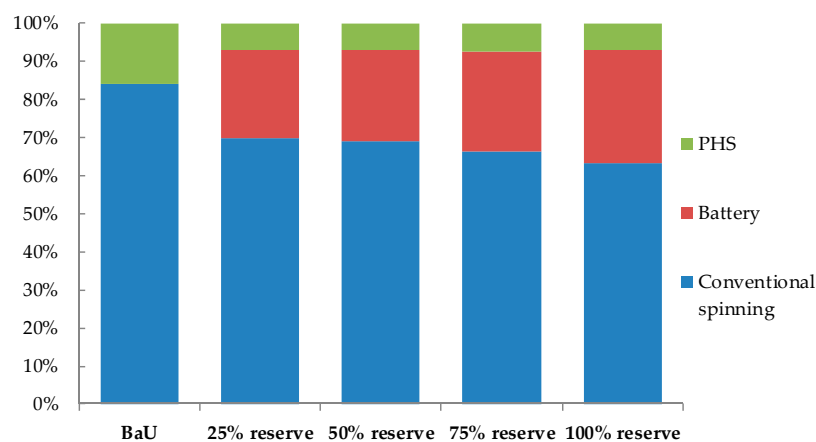


Figure 21. Secondary up reserve provision contribution from different technologies (“integrated B”).

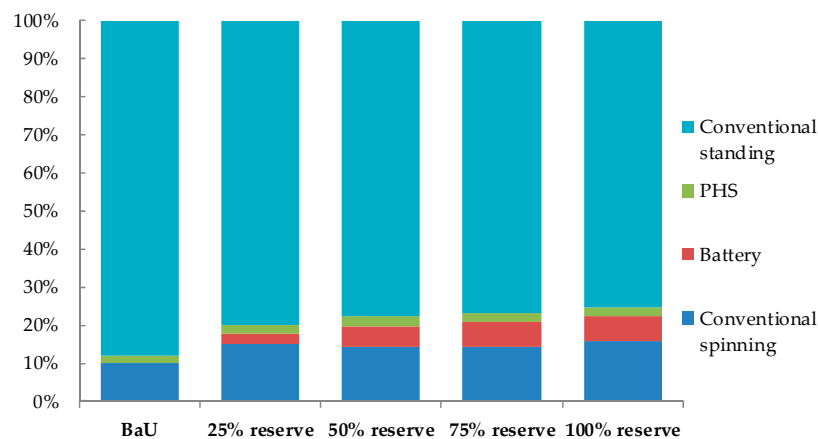


Figure 22. Tertiary up reserve provision contribution from different technologies (“integrated B”).

4.4. Capacity Credit of DES and PV

The four capacity credit metrics are presented in Figure 23. As seen in Figure 23, “integrated” control exhibits a much higher capacity credit (measured by all four metrics) over “independent” control. In addition, “independent” control leads to saturation, whereas the “integrated” control shows a sustained linear increase following an increase in battery energy capacity. This is due to two reasons. Firstly, under the “integrated” control approach batteries are controlled with consideration of all the generation sources in the system, particularly wind availability. In other words, “integrated” control can enable batteries at peak times to complement wind generation and thus leads to a higher contribution to system capacity, whereas “independent” control only stores the solar energy generated in the daytime to minimise the system peak demand in the evening. This is why batteries have higher capacity credit under “integrated” control than batteries under “independent” control even before the saturation. Secondly, the capacity credit of batteries under “integrated” control does not saturate, due to the fact that they could be charged by all generation sources, allowing a sustained increase in the contribution to peak reduction; whereas, under “independent” control, batteries could only shift the energy production from the PV panels to supply the peak demand, such that the contribution to generation capacity is limited by the output from PV panels during winter days.

In terms of different capacity credit metrics, according to Figure 23a, the ELCC metric indicates that each additional 500 MW with 1 GWh energy capacity of batteries can withstand a demand increase of 190 MW under “Integrated” control; while under “Independent” control it is 81 MW before saturation. The EFC in Figure 23b shows that each additional 500 MW with 1 GWh energy capacity of batteries is equivalent to an additional generation capacity of 213 MW that is available at all times under the “integrated” control; while under “independent” control it is 94 MW before saturation. It is worth pointing out, as seen in Figure 23c, when a CCGT is chosen as the real generator in the assessment, a CCGT with the attached reliability characteristic cannot provide a measurement of the ECC metric for the energy capacity of batteries over 5 GW with 10 GWh energy capacity under “integrated” control. This is because as seen in Figure 10c the adequacy level of the system without DES provided by the additional CCGT capacity will saturate before it can reach the adequacy level provided by the corresponding DES. It can also be seen in Figure 23c that the contribution from approximately 5 GW with 10 GWh of energy capacity of batteries to system adequacy of supply is equivalent to a 5 GW CCGT under “integrated” control. However, under “independent” control the value is only slightly more than a 1 GW CCGT. Finally, the EGCS in Figure 23d demonstrates clearly that each additional 500 MW with 1 GWh of energy capacity of batteries can displace 196 MW of CCGT under “integrated” control, while under “independent” control the maximum CCGT that can be displaced is a bit less than 2 GW.

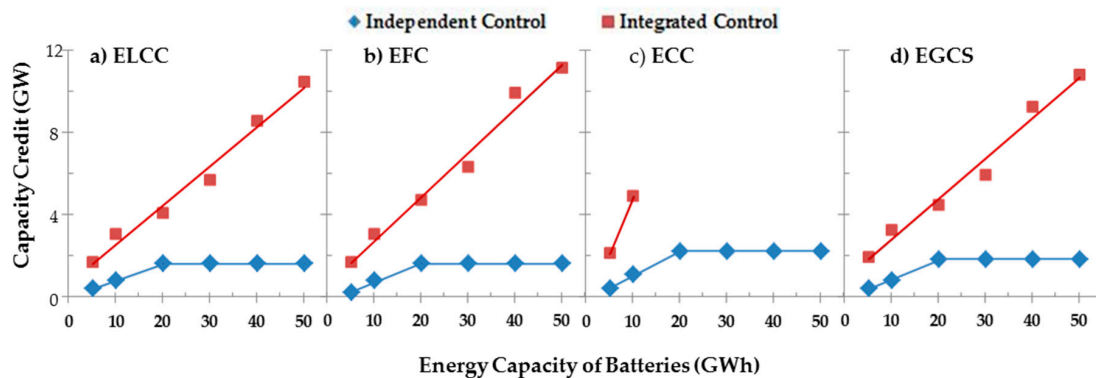


Figure 23. Capacity credit metrics (in GW) assessed for “independent” control and “integrated” control at different penetration levels of batteries: (a) ELCC; (b) EFC; (c) ECC; (d) EGCS.

In addition to the absolute value of the different capacity credit metrics, Figure 24 presents the capacity credit as a percentage of the corresponding maximum discharging rate of all the batteries installed in the system (i.e., aggregated power capacity). It is worth highlighting that under “integrated” control the ELCC, EFC and EGCS metrics all exhibit a decreasing trend following an increase of the battery penetration level, apart from the ECC metric. This is because the reliability characteristics of the CCGT used to evaluate ECC cause the equivalent CCGT capacity to increase rapidly and surpass the corresponding aggregated power capacity of the batteries. This implies that the effectiveness of using batteries to contribute to generation capacity under “integrated” control declines significantly as the battery penetration level increases, although the capacity credit in GW keeps increasing (as seen in Figure 24). However, under “independent” control, the capacity credit (%) increases slightly before decreasing due to saturation, as shown in Figure 24. It is also important to observe that the capacity credit (%) under “integrated” control tends to saturate to a value close to 40%. Note that the ECC metric (%) is an exception for the above discussion, due to the imperfectly reliable generator that has been chosen for the corresponding assessment.

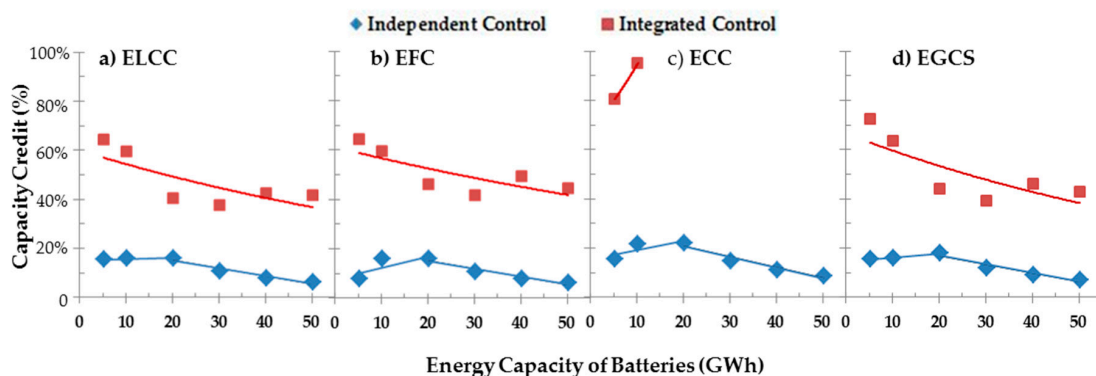


Figure 24. Capacity credit metrics (% maximum discharging rate) assessed for “independent” control and “integrated” control at different penetration levels of batteries: (a) ELCC; (b) EFC; (c) ECC; (d) EGCS.

Based on the above values obtained for the capacity credit metrics, the following system-level implications can be drawn, namely:

- Solar PV in conjunction with DES is capable of contributing to system adequacy; however, this capacity contribution is eventually limited by the amount of solar energy that will typically be available on days with critical peak demands. In the case of the GB system, due to the

natural characteristics of solar energy sources, and underlying load patterns, the capacity credit of solar PV coordinated with DES represented by all four metrics (that is, in terms of demand increase, generation capacity available all the time, equivalent CCGT capacity or displaced CCGT capacity) can only reach close to 2 GW, corresponding to a PV penetration level of 34.6 GW and an associated battery energy capacity of 20.2 GWh (i.e., a power capacity of 10.1 GW according to the assumption that all the batteries have a maximum charging rate of 5 kW and an energy capacity of 10 kWh).

- There is an intrinsic capacity credit for DES, although it is not controlled for the provision of system capacity. In particular, because the DES can be charged from all energy sources, the capacity contribution is higher than that when DES only shifts PV generation. This is an important finding as it clearly demonstrates that there will be an inherent capacity contribution from distributed batteries while they are providing reserve services to the system. As a further point, whether DES is controlled to shift PV generation or it is controlled in a broader manner to provide support to system operation, the DES control needs to be coordinated (or incentivised) by the system operator in order to contribute to system capacity.

In terms of the application of different capacity credit metrics, as defined in Section 2.7, the ELCC metric is generally used for system expansion in the presence of load growth; the EFC and ECC metrics are used to compare the capacity contribution from the proposed DES-enabled system with the capacity contribution from a conventional generation resource (e.g., using EFC if comparing to a perfect generation unit or using ECC if comparing to a “real” generation unit); finally, the EGCS metric is defined to represent the capability of the proposed DES-enabled system to replace existing generation. Within the context of the case study, application of the ELCC and EGCS metrics may thus be more practical. This is because the system may face potential load growth due to electrification of transport and heating, while displacing existing conventional generators with the proposed DES-enabled system is in line with the overall environmental target for the GB power system.

5. Conclusions

This paper has investigated the system-level impacts of PV and DES from both operational and adequacy perspectives, assessing, in particular, the benefits of utilising DES to support the operation of a system with high penetration of renewable generation, particularly PV. Models of different DES control strategies have been developed for different operational objectives and then integrated into a fast unit commitment model based on linear programming which includes multiple ancillary services and consideration for system inertia. Interconnection is also modelled in order to understand its flexibility contribution on system operation. Additionally, a dynamic reserve allocation method has been proposed to optimise renewable generation integration and reserve provision. In parallel to these operational analyses, a framework for assessing the capacity credit of DES and PV systems has been developed with different definitions of capacity credit metrics and corresponding assessment algorithms.

Specific case studies have been carried out based on scenarios for the GB power system in 2035, where an increase in electricity consumption due to the electrification of heating and transport sectors has also been considered. The analysis has been carried out from several different perspectives. Firstly, the pros and cons of adding extra PV capacity to system operation have been analysed. Then, the value of interconnectors in providing flexibility has been examined by limiting their import and export capacity. Finally, the impacts of two different DES control strategies have been evaluated from both operational and adequacy perspectives, where DES is not only participating in energy arbitrage but also being utilised to provide portfolio reserve services in order to minimise the system operational cost.

Based on the findings, the 2035 GB system might experience in the order of 14 TWh of annual wind generation curtailment (13.4%). In recognition of such high wind curtailment, the scenario might not materialise as it might not be effective to add wind capacity into a system that is not sufficiently flexible. On the other hand, if wind generation was to participate in the provision of frequency control

ancillary services, wind farms could accrue economic benefits not only from their energy production but also from their contribution to system flexibility. This might thus sustain the interest in investing in wind generation, in spite of potentially curtailed energy. At the same time, as the flexibility of the system could increase owing to the system support from wind farms, the level of generation curtailment could decrease too.

Increasing the amount of DES for energy arbitrage purposes only brings limited benefits for renewable energy integration, as the system is still too inflexible and cannot fully accommodate the renewable generation at the scheduling stage due to lack of ancillary service provision capability. Therefore, it is necessary to increase the system flexibility in terms of ancillary service provision as well, and this lack of flexibility could potentially lead to investment in new flexibility providers. In this respect, DES providing reserves results in considerable reduction of the total wind curtailment. For example, wind curtailment drops from 14 TWh to 1 TWh in the “integrated B” scenario, which demonstrates the substantial benefits of the flexibility contribution from batteries for multiple services and different time-scales. However, the volume of additional flexibility requirement is limited, when it is used to improve certain aspects of system operation. For example, there is no further wind curtailment reduction when batteries are allowed to use all their capacity to provide ancillary services comparing with a 50% case, as the amount of renewable generation that can be integrated is also limited by the system minimum stable generation level due to inflexible nuclear plants. This fact points out that policies pushing for both high RES and baseload nuclear may be in conflict and lead to operational and market issues, so that a careful review might be required.

In parallel to the aforementioned operational findings, it is clearly seen from the capacity credit assessment that: on one hand, with the help of DES, PV is able to make a limited amount of contribution to system capacity, and the amount of DES that is needed in this perspective has a clear upper boundary; on the other hand, although DES is not controlled for the specific purpose of contributing to system capacity, it is found that DES still has a substantial intrinsic capacity value to the system. More specifically, the capacity credit of DES (in GW) follows a linear relationship with the energy capacity of DES under both “integrated” and “independent” controls. However, in the case of “independent” Control, the capacity credit of DES exhibits a clear saturation due to fact that DES can only shift PV generation. In addition to the capacity credit in GW, the capacity credit as a percentage of the power capacity of DES shows a significant decreasing trend following an increase of DES total energy capacity in the case of “integrated” control, whereas under “independent” control the capacity credit in percentage increases slightly before the decline due to saturation of the capacity credit. This implies that under “integrated” control the effectiveness of DES for the provision of system capacity does not increase following an increase in the number of DES systems.

Future work can be constituted of two parts: (1) simulating the operation of individual power plants at high renewable energy penetration levels and exploring the balance of system scheduling decisions between low operational cost generators and highly flexible plants; (2) extending the possibility of providing ancillary services to other (market) entities, such as renewable generation and demand response, in order to give a comprehensive assessment of the flexibility available in the system.

Acknowledgments: The authors thank the support by the UK EPSRC in the WISE-PV project (EP/K022229/1), the MY-STORE project (EP/N001974/1), and the Newton-Picarte “Disaster management and resilience in electric power systems” project (EP/N034899/1), under which this research has been conducted.

Author Contributions: This paper has been written by Lingxi Zhang, Yutian Zhou, Damian Flynn, Joseph Mutale, and Pierluigi Mancarella. Lingxi Zhang wrote the main part and worked on the specific aspects of the unit commitment model. Yutian Zhou provided the studies on DES control and capacity credit assessment. Damian Flynn provided advice on technical details of modelling and discussion of results, as well as internal review. Joseph Mutale provided internal review and feedback regarding the discussion of the results and the corresponding higher level implications. Pierluigi Mancarella proposed the original idea, gave guidance on technical modelling and paper structure, and provided technical feedback and internal review.

Conflicts of Interest: The authors declare no conflict of interest.

Glossary

BaU	Business as usual
CCGT	Combined cycle gas turbine
DES	Distributed energy storage
ECC	Equivalent conventional capacity
EFC	Equivalent firm capacity
EGCS	Equivalent generation capacity substituted
EHP	Electric heat pump
ELCC	Effective load carrying capability
EV	Electric vehicle
GB	Great Britain
HVDC	High voltage, direct current
LOLF	Loss of load frequency
LP	Linear programming
MIP	Mixed integer programming
OCGT	Open cycle gas turbine
Ofgem	Office of gas and electricity markets
PFR	Primary frequency response
PHS	Pumped hydro storage
PV	Photovoltaic
QSS	Quasi-steady-state
RoCoF	Rate of change of frequency
SMCS	Sequential Monte-Carlo simulation
STOR	Short term operating reserve
UC	Unit commitment

Nomenclature

i, I	reserve service, set of reserve services
l, L	interconnector cluster, set of interconnector clusters
m, M	distributed energy storage cluster, set of distributed energy storage clusters
n, N	generator cluster, set of generator clusters
s, S	pumped hydro storage cluster, set of pumped hydro storage clusters
t, τ, T	time step (h), sub-time-step (s), set of time steps
Δ^{ts}	simulation time step interval (h)
Δ_i^r	reserve provision sustain period (h)
$bn_{m,t}^{DES}$	distributed energy storage operating mode (1 represents charging mode and 0 represents discharging mode)
$bn_{l,t}^{int}$	interconnector operating mode (1 represents import mode and 0 represents export mode)
C_n^{conNL}	conventional generator no load cost (£/h)
$C_{x,n,t}^{conOP}$	conventional generator segment output fuel cost (£/MWh)
$C^{curtw/ps}$	wind/solar generation curtailment cost (£/MWh)
C^{shed}	load shedding cost (£/MWh)
$C_l^{int_{im/ex}}$	import/export electricity price of interconnector (£/MWh)
$CL^{int_{im/ex}}$	export/export capacity limit of interconnector (%)
d_t^{Ap}	domestic appliances load reduction (MW)
d_t^{EHP}	demand of electric heat pumps (MW)
d_t^{EV}	demand of electric vehicles (MW)
d_t^{shed}	system load shedding (MW)
D_t	system demand (MW)
D_t^F	future system demand (MW)
D_t^C	current system demand (MW)

D_{pr}	load damping rate (1/Hz)
E_t^{sys}	system stored rotational energy (MW·s)
$e_{m,t}^{DES}$	energy level of distributed energy storage (MWh)
e_{C^*}	daily minimum consumption of households from grid side (MWh)
$E_m^{DES_{Max/Min}}$	maximum and minimum energy level of distributed energy storage (MWh)
frr_t	primary frequency response provision rate requirement (MW)
$\Delta f_{t+\tau}^{sys}$	system frequency change at sub-time-step (Hz)
f_{t+0}^{sys}	system nominal frequency (Hz)
Δf^{db}	frequency deadband before triggering frequency response provision (Hz)
Δf^{Nadir}	nadir frequency drop (Hz)
$\Delta f^{QSS_{Max}}$	quasi-steady-state frequency deviation allowance (Hz)
FR_n^{Max}	maximum primary frequency response provision capability of conventional generator (MW)
H_n^{con}	inertia value of conventional generator (MW·s/MVA)
$H^{loss_{Max}}$	inertia value of maximum infeed generator (MW·s/MVA)
H_s^{phs}	inertia value of pumped hydro storage (MW·s/MVA)
K	daily peak demand of households (MW)
$K^{original}$	original daily peak power of households (MW)
K^*	minimum daily peak power of households (MW)
$p_{n,t}^{con}$	conventional generator cluster output power (MW)
$p_{m,t}^{DES}$	distributed energy storage output power (MW)
$p_{m,t}^{DES_{c/dc}}$	charging/discharging power of distributed energy storage (MW)
$p_{m,t}^{FI}$	household feed-in power (MW)
$p_{m,t}^G$	household electricity consumption from grid side (MW)
$p_{l,t}^{int}$	interconnector equivalent import power (MW)
$p_{l,t}^{int_{im/ex}}$	import/export power of interconnector cluster (MW)
p_m^{MFI}	maximum household feed-in power (MW)
p_s^{phs}	pumped hydro storage equivalent output (MW)
$P_n^{con_{Max/Min}}$	conventional generator maximum/minimum output (MW)
$p^{DES_{Max/Min}}$	maximum and minimum output of distributed energy storage (MW)
$p^{int_{Max}}$	power capacity of interconnector (MW)
$p_s^{phs_{Max}}$	pumped hydro storage power capacity (MW)
$p^{loss_{Max}}$	capacity of the maximum generator in the system (MW)
p_t^{loss}	generation loss (MW)
$p_{v,m,t}$	PV panel integrable output (MW)
$PV_{m,t}$	PV panel potential output (MW)
$r_{n,t}^{con}$	reserve provision from conventional generator cluster (MW)
$r_{m,i,t}^{DES_{up/dn}}$	upward/downward reserve provision from distributed energy storage (MW)
$r_{s,i,t}^{phs}$	reserve provision from pumped hydro storage cluster (MW)
$r_{i,t}^{UP/DN}$	secondary and tertiary upward/downward reserve requirement (MW)
RP^{DES}	distributed energy storage reserve provision capacity limit (%)
$ROCOF^{Max}$	maximum rate of change of frequency allowance (Hz/s)
RAM_{l}^{pint}	interconnector maximum ramping rate (MW/h)
$RAM_{n}^{con_{up/dn}}$	conventional maximum upward/downward ramping rate (MW/h)
T^d	frequency response delivery time (s)
$T_n^{UP/DN}$	minimum up/down time of conventional generators (h)
$U_{n,t}^{con}$	online units of conventional generator cluster
$U_{n,t}^{con_{ST/SD}}$	start-up/shut-down units in a conventional generator cluster
$U_{s,t}^{phs}$	online units of pumped hydro storage cluster
W_t	wind forecast output (MW)

ω_t	wind curtailment at scheduling stage (MW)
w_t	wind integrable output (MW)
α^{fr}	frequency response function slope ratio
$\delta_i^{W/S}$	forecast error standard deviation percentage of wind and solar forecast output (%)
$\eta^{DES_{c/dc}}$	charging/discharging efficiency of distributed energy storage (%)
χ_t	pv generation curtailment (MW)
β^{pf}	ratio of active power (MW) rating to apparent power (MVA) equipment rating

Appendix A

The constraints of the LP UC model introduced in [31] are listed as follows. The objective function is to minimise the system operational cost, as depicted in (A1). The energy balance of solar PV generation is described in (A2). The energy balance of the system is determined in (A3). The primary frequency response and secondary and tertiary upward and downward reserves are provided by a group of conventional generators, PHS and DES, as given in (A4) and (A5). The primary frequency response provision from a conventional generator cluster is limited by its maximum provision capability, as shown in (A6). Moreover, the reserve provision capability is constrained by the ramping rate of conventional generators and the headroom of upward and downward ramping as given in (A7)–(A9). The online unit of a conventional generator cluster is calculated with the number of starting-up/shutting down units at each time step in (A10). Further, the minimum up and down times of conventional generators restrict the start-up and shut down activities of generators, as shown in (A11) and (A12). Changes in output of conventional generators is also limited by their ramping rates, their headroom, and the number of units starting up or shutting down, as illustrated in (A13)–(A15).

$$\text{Minimise } \left\{ \sum_{t \in T} \sum_{n \in N} \left[\left(C_n^{con_{NL}} \cdot U_{n,t}^{con} + p_{n,t}^{con} \cdot C_{n,t}^{con_{OP}} \right) \cdot \Delta^{ts} + C_n^{con_{ST}} \cdot U_{n,t}^{con_{ST}} + \left(C^{shed} \cdot d_t^{shed} + C^{curt_w} \cdot \omega_t + C^{curt_{pv}} \cdot \chi_t + \sum_{l \in L} \left(p_{l,t}^{int_{im}} \cdot C_l^{int_{im}} - p_{l,t}^{int_{ex}} \cdot C_l^{int_{ex}} \right) \right) \cdot \Delta^{ts} \right] \right\} \quad (\text{A1})$$

$$\chi_t + \sum_{m \in M} pv_{m,t} = \sum_{m \in M} PV_{m,t} \quad (\text{A2})$$

$$w_t + pv_t + \sum_{n \in N} p_{n,t}^{con} + \sum_{s \in S} p_{s,t}^{phs} + \sum_{l \in L} p_{l,t}^{int} + \sum_{m \in M} p_{m,t}^{DES} = D_t - d_t^{shed} \quad (\text{A3})$$

$$frr_t \leq \sum_{n \in N} frr_{n,t}^{con} \quad (\text{A4})$$

$$r_{i,t}^{UP/DN} \leq \sum_{n \in N} r_{n,i,t}^{con_{up/dn}} + \sum_{s \in S} r_{s,i,t}^{phs_{up/dn}} + \sum_{m \in M} r_{m,i,t}^{DES_{up/dn}} \quad (\text{A5})$$

$$frr_{n,t}^{con} \cdot T_d \leq U_{n,t}^{con} \cdot FR_n^{Max} \quad (\text{A6})$$

$$r_{n,i,t}^{con_{up/dn}} \leq RAMP_{n,t}^{con_{up/dn}} \cdot U_{n,t}^{con} \cdot \Delta_i^r \quad \forall i \in I \quad (\text{A7})$$

$$\sum_{i \in I} r_{n,i,t}^{con_{up}} + \frac{frr_{n,t}^{con} \cdot T_d}{\alpha^{fr}} \leq P_n^{con_{Max}} \cdot U_{n,t}^{con} - p_{n,t}^{con} \quad (\text{A8})$$

$$\sum_{i \in I} r_{n,i,t}^{con_{dn}} \leq p_{n,t}^{con} \quad (\text{A9})$$

$$U_{n,t}^{con} - U_{n,t-1}^{con} = U_{n,t}^{con_{ST}} - U_{n,t}^{con_{SD}} \quad (\text{A10})$$

$$U_{n,t}^{con} \leq G_n - \sum_{\beta \in [1,t-(T_n^{DN}-1)]} U_{n,\beta}^{con_{SD}} \quad (\text{A11})$$

$$U_{n,t}^{con} \geq \sum_{\beta \in [1,t-(T_n^{UP}-1)]} U_{n,\beta}^{con_{ST}} \quad (\text{A12})$$

$$p_{n,t}^{con} - p_{n,t-1}^{con} \leq U_{n,t}^{con} \cdot RAMP_n^{con_{up}} \cdot \Delta^{ts} + U_{n,t}^{con_{ST}} \cdot P_n^{con_{Min}} \quad (A13)$$

$$p_{n,t}^{con} \leq U_{n,t-1}^{con} \cdot P_n^{con_{Max}} + U_{n,t}^{con_{ST}} \cdot P_n^{con_{Min}} \quad (A14)$$

$$p_{n,t-1}^{con} - p_{n,t}^{con} \leq U_{n,t}^{con} \cdot RAMP_n^{con_{dn}} \cdot \Delta^{ts} + U_{n,t}^{con_{SD}} \cdot P_n^{con_{Min}} \quad (A15)$$

References

1. *The Paris Agreement*; United Nations: Paris, France, 2015; pp. 1–27.
2. Hemingway, J.; Waters, L. *Energy Trends: Renewables*; Department of Business Energy & Industrial Strategy: London, UK, 2016.
3. Future Energy Scenarios: GB Gas and Electricity Transmission. Available online: http://media.nationalgrid.com/media/1169/future_energy_scenarios_2015.pdf (accessed on 7 July 2017).
4. *Next Generation Wind and Solar Power*; IEA: Paris, France, 2016.
5. Muenzel, V.; Mareels, I.; De Hoog, J.; Vishwanath, A.; Kalyanaraman, S.; Gort, A. PV generation and demand mismatch: Evaluating the potential of residential storage. In Proceedings of the 2015 IEEE Power & Energy Society Innovative Smart Grid Technologies Conference (ISGT), Washington, DC, USA, 18–20 February 2015.
6. Sarker, M.R.; Ortega-vazquez, M.A. Optimal investment strategy in photovoltaics and energy storage for commercial buildings. In Proceedings of the 2015 IEEE Power & Energy Society General Meeting, Denver, CO, USA, 26–30 July 2015.
7. Teng, J.H.; Luan, S.W.; Lee, D.J.; Huang, Y.Q. Optimal charging/discharging scheduling of battery storage systems for distribution systems interconnected with sizeable PV generation systems. *IEEE Trans. Power Syst.* **2013**, *28*, 1425–1433. [CrossRef]
8. Alam, M.J.E.; Muttaqi, K.M.; Sutanto, D. Mitigation of rooftop solar PV impacts and evening peak support by managing available capacity of distributed energy storage systems. *IEEE Trans. Power Syst.* **2013**, *28*, 3874–3884. [CrossRef]
9. Nottrott, A.; Kleissl, J.; Washom, B. Storage dispatch optimization for grid-connected combined photovoltaic-battery storage systems. In Proceedings of the 2012 IEEE Power and Energy Society General Meeting, San Diego, CA, USA, 22–26 July 2012.
10. Ru, Y.; Kleissl, J.; Martinez, S. Storage size determination for grid-connected photovoltaic systems. *IEEE Trans. Sustain. Energy* **2013**, *4*, 68–81. [CrossRef]
11. Taheri, H.; Akhrif, O.; Okou, A.F. Contribution of PV generators with energy storage to grid frequency and voltage regulation via nonlinear control techniques. In Proceedings of the IECON 2013—39th Annual Conference of the IEEE Industrial Electronics Society, Vienna, Austria, 10–13 November 2013.
12. Lew, D.; Piwko, R. *Western Wind and Solar Integration Study: Hydropower Analysis*; National Renewable Energy Laboratory: Golden, CO, USA, 2012.
13. Denholm, P.; Margolis, R. *Energy Storage Requirements for Achieving 50% Solar Photovoltaic Energy Penetration in California*; National Renewable Energy Laboratory: Golden, CO, USA, 2016.
14. National Grid Historic Demand Data. Available online: <http://www2.nationalgrid.com/UK/Industry-information/Electricity-transmission-operational-data/Data-Explorer/> (accessed on 1 January 2017).
15. Teng, F.; Trovato, V.; Strbac, G. Stochastic scheduling with inertia-dependent fast frequency response requirements. *IEEE Trans. Power Syst.* **2016**, *31*, 1557–1566. [CrossRef]
16. Foley, A.M.; Leahy, P.; McKeogh, E.J. Wind energy integration and the Ireland-Wales interconnector. In Proceedings of the 2009 IEEE PES/IAS Conference on Sustainable Alternative Energy (SAE), Valencia, Spain, 28–30 September 2009; pp. 1–6.
17. Richardson, N.; Alexander, M.J.; James, P. Energy storage against interconnection as a balancing mechanism for a 100% renewable UK electricity grid. *IET Renew. Power Gener.* **2015**, *9*, 131–141. [CrossRef]
18. Panteli, M.; Mancarella, P. The grid: Stronger, bigger, smarter?: Presenting a conceptual framework of power system resilience. *IEEE Power Energy Mag.* **2015**, *13*, 58–66. [CrossRef]
19. Holttinen, H.; Milligan, M.; Ela, E.; Menemenlis, N.; Dobschinski, J.; Rawn, B.; Bessa, R.J.; Flynn, D.; Gomez-Lazaro, E.; Detlefsen, N.K. Methodologies to determine operating reserves due to increased wind power. *IEEE Trans. Sustain. Energy* **2012**, *3*, 713–723. [CrossRef]

20. Ela, E.; Milligan, M.; Kirby, B. Operating Reserves and Variable Generation. Available online: <http://www2.econ.iastate.edu/tesfatsi/OperatingReservesVariableGenerationSurvey.NRELAug2011.pdf> (accessed on 5 July 2017).
21. Delille, G.; François, B.; Malarange, G. Dynamic frequency control support by energy storage to reduce the impact of wind and solar generation on isolated power system's inertia. *IEEE Trans. Sustain. Energy* **2012**, *3*, 931–939. [[CrossRef](#)]
22. Rezkalla, M.; Marinelli, M.; Pertl, M.; Heussen, K. Trade-off analysis of virtual inertia and fast primary frequency control during frequency transients in a converter dominated network. In Proceedings of the 2016 IEEE Innovative Smart Grid Technologies-Asia (ISGT-Asia), Melbourne, Australia, 28 November–1 December 2016.
23. Pudjianto, D.; Aunedi, M.; Djapic, P.; Strbac, G. Whole-systems assessment of the value of energy storage in low-carbon electricity systems. *IEEE Trans. Smart Grid* **2014**, *5*, 1098–1109. [[CrossRef](#)]
24. Daneshi, H.; Srivastava, A.K. Security-constrained unit commitment with wind generation and compressed air energy storage. *IET Gener. Transm. Distrib.* **2012**, *6*, 167–175. [[CrossRef](#)]
25. Munoz, F.D.; Mills, A.D. Endogenous assessment of the capacity value of solar PV in generation investment planning studies. *IEEE Trans. Sustain. Energy* **2015**, *6*, 1574–1585. [[CrossRef](#)]
26. Madaeni, S.H.; Sioshansi, R.; Denholm, P. Comparing capacity value estimation techniques for photovoltaic solar power. *IEEE J. Photovolt.* **2013**, *3*, 407–415. [[CrossRef](#)]
27. Duignan, R.; Dent, C.J.; Mills, A.; Samaan, N.; Milligan, M.; Keane, A.; O'Malley, M. Capacity value of solar power. In Proceedings of the 2012 IEEE Power and Energy Society General Meeting, San Diego, CA, USA, 22–26 July 2012.
28. Huang, Y.; Liu, C.; He, G.; Xu, X.; He, J.; Wang, W.; Zhou, X. Capacity value of PV generation and its impact on power system planning: A case study in northwest of China. In Proceedings of the 2010 Asia-Pacific Power and Energy Engineering Conference (APPEEC), Chengdu, China, 28–31 March 2010.
29. Good, N.; Zhang, L.; Navarro-Espinosa, A.; Mancarella, P. High resolution modelling of multi-energy domestic demand profiles. *Appl. Energy* **2015**, *137*, 193–210. [[CrossRef](#)]
30. Grahm, P.; Munkhammar, J.; Widen, J.; Alvehag, K.; Soder, L. PHEV home-charging model based on residential activity patterns. *IEEE Trans. Power Syst.* **2013**, *28*, 2507–2515. [[CrossRef](#)]
31. Zhang, L.; Capuder, T.; Mancarella, P. Unified unit commitment formulation and fast multi-service LP model for flexibility evaluation in sustainable power systems. *IEEE Trans. Sustain. Energy* **2016**, *7*, 658–671. [[CrossRef](#)]
32. Feizollahi, M.J.; Costley, M.; Ahmed, S.; Grijalva, S. Large-scale decentralized unit commitment. *Int. J. Electr. Power Energy Syst.* **2015**, *73*, 97–106. [[CrossRef](#)]
33. Pandzic, H.; Ting, Q.; Kirschen, D.S. Comparison of state-of-the-art transmission constrained unit commitment formulations. In Proceedings of the 2013 IEEE Power and Energy Society General Meeting, Vancouver, BC, Canada, 21–25 July; pp. 1–5.
34. Morales-España, G.; Latorre, J.M.; Ramos, A. Tight and compact MILP formulation for the thermal unit commitment problem. *IEEE Trans. Power Syst.* **2013**, *28*, 4897–4908. [[CrossRef](#)]
35. Ulbig, A.; Borsche, T.S.; Andersson, G. Impact of low rotational inertia on power system stability and operation. *IFAC Proc.* **2014**, *19*, 7290–7297. [[CrossRef](#)]
36. Halamay, D.A.; Brekken, T.K.A.; Simmons, A.; McArthur, S. Reserve requirement impacts of large-scale integration of wind, solar, and ocean wave power generation. *IEEE Trans. Sustain. Energy* **2011**, *2*, 321–328. [[CrossRef](#)]
37. Guizzi, G.L.; Iacovella, L.; Manno, M. Intermittent non-dispatchable renewable generation and reserve requirements: Historical analysis and preliminary evaluations on the Italian electric grid. *Energy Procedia* **2015**, *81*, 339–344. [[CrossRef](#)]
38. Black, M.; Strbac, G. Value of bulk energy storage for managing wind power fluctuations. *IEEE Trans. Energy Convers.* **2007**, *22*, 197–205. [[CrossRef](#)]
39. Zhou, Y.; Mancarella, P.; Mutale, J. Modelling and assessment of the contribution of demand response and electrical energy storage to adequacy of supply. *Sustain. Energy Grids Netw.* **2015**, *3*, 12–23. [[CrossRef](#)]
40. Zhou, Y.; Mancarella, P.; Mutale, J. Framework for capacity credit assessment of electrical energy storage and demand response. *IET Gener. Transm. Distrib.* **2016**, *10*, 2267–2276. [[CrossRef](#)]

41. *Implementing Electricity Market Reform (EMR)*; Department of Energy and Climate Change: London, UK, 2014.
42. Nolan, S.; O'Malley, M.; Hummon, M.; Kiliccote, S.; Ma, O. A methodology for estimating the capacity value of demand response. In Proceedings of the 2014 IEEE PES General Meeting, Conference & Exposition, National Harbor, MD, USA, 27–31 July 2014.
43. *Changes to the Distribution Code and Engineering Recommendation G59: Frequency Changes during Large Disturbances and Their Impact on the Total System*; Office of Gas and Electricity Markets: London, UK, 2014; pp. 1–8.
44. Reedy, B. Utility Needs of Power Conditioning Systems for PV and other Renewable DG—A New Twist. Available online: https://www.nist.gov/sites/default/files/documents/pml/high_megawatt/Reedy.pdf (accessed on 5 July 2017).
45. Zhou, Y.; Mancarella, P.; Mutale, J. Generation adequacy in wind rich power systems: Comparison of analytical and simulation approaches. In Proceedings of the 2014 International Conference on Probabilistic Methods Applied to Power Systems (PMAPS), Durham, UK, 7–10 July 2014; pp. 1–6.
46. Costs and Benefits of GB Interconnection. Available online: https://www.gov.uk/government/uploads/system/uploads/attachment_data/file/505222/080_Poyry_CostsAndBenefitsOfGBInterconnection_v500.pdf (accessed on 5 July 2017).



© 2017 by the authors. Licensee MDPI, Basel, Switzerland. This article is an open access article distributed under the terms and conditions of the Creative Commons Attribution (CC BY) license (<http://creativecommons.org/licenses/by/4.0/>).